Long term evolution of the spin of Venus - II. Numerical simulations.

Alexandre C.M. Correia and Jacques Laskar

Astronomie et Systèmes Dynamiques, IMC-CNRS UMR8028,

77 Av. Denfert-Rochereau, 75014 Paris, France

Abstract

We present here the numerical application of the theoretical results derived in Correia *et al.* (2002) for the spin evolution of Venus since its formation. We explore a large variety of initial conditions in order to cover the possible formation and evolutionary scenarios. In particular, we pay a special attention to the evolutions which cross the chaotic zone resulting from secular planetary perturbations (Laskar and Robutel, 1993). We demonstrate that Venus' axis can be temporarily trapped in a secular resonance with the node of Neptune's orbit, which can prevent it from being tilted to 180°, and will drive it towards 0°. We test several dissipation models and parameters to evaluate their contribution to the planet's spin history. We confirm that despite the variations in the models, only three of the four final spin states of Venus are possible (Correia and Laskar, 2001) and that the present observed retrograde spin state of Venus can be attained by two different processes. In the first scenario ($\mathcal{F}_\pi^-$), the axis is tilted towards 180° while its rotation rate slows down, while in the second one, the axis is driven towards 0° obliquity and the rotation rate decreases, stops, and increases again in the reverse direction to a final equilibrium value ($\mathcal{F}_0^-$).

Key Words: Venus; obliquity; spin dynamics; resonances; chaos.

1   Introduction

The present rotation of Venus may represent a steady state under the influence of gravitational and atmospheric tides (Gold and Soter, 1969) and core-mantle friction (Goldreich and Peale, 1970) after a long evolutionary process (eg. Dobrovolskis, 1980). Laskar and Robutel (1993) have shown that, due to planetary perturbations, there exists a large chaotic zone for the spin of each terrestrial planet. The passage of Venus in this chaotic zone allows the spin axis to be tilted to 180° starting with any initial obliquity (Laskar and Robutel, 1993, Néron de Surgy, 1996, Yoder, 1997). Finally, Correia and Laskar (2001, hereafter

referred as V1) have shown that most initial conditions lead Venus to its present configuration, though by two completely different processes. In (Correia *et al.*, 2002, referred as V2) we presented a detailed description of the equations governing the spin evolution of Venus, including planetary perturbations and dissipative effects. We analyzed the possible evolution scenarios and the constraints on the dissipation models and parameters.

The present paper is devoted to the analysis of extended numerical simulations of Venus' spin evolution. We will first choose a set of plausible coefficients for the models defined in (V2), and we will call it the 'standard model'. For some of the dissipative parameters, when their values for Venus are unknown, we will use the Earth values (assuming that the internal structures of these two planets are similar). In some other cases, we will use the constraints imposed by the necessity for the planet to evolve into the present configuration within the age of the Solar System (4.6 Ga). The standard model is presented in the next section, where our parameter choices are justified. Using this model, massive numerical integrations are done, with and without planetary perturbations in order to cover all possible scenarios, starting with any initial condition. In section three, we analyze the deviations from the standard model resulting from different tidal and core-mantle friction models, as well as the effect of a late formation of the atmosphere. In section four we explore other models and the last section is devoted to the conclusions. In all the following, we kept the notations and symbols from the companion paper (V2).

2   The standard model

2.1   Choice of the parameters

Some of the parameters related to the dissipation have actually been measured for Venus or for the Earth. As these two planets have similar sizes and mean densities, it is conceivable that their internal structure and composition are not very different. This will allow us to use the Earth parameters when the corresponding Venus quantities are unknown. Among the well-known data are the

mass, the mean radius and the mean density of Venus, respectively (McNamee *et al.*, 1993): $m = 4.8685 \times 10^{24}$Kg, $R = 6.0518 \times 10^6$m and $\bar{\rho} = 5.204\,\text{g cm}^{-3}$. The potential Love number is (Konopliv and Yoder, 1996): $k_2 = 0.295 \pm 0.066$. The present parameters of the Venusian atmosphere are also known, though less accurately than the previous ones. The specific heat at constant pressure, the mean ground temperature and the solar flux absorbed by the ground, are respectively (Avduevskii *et al.*, 1976): $c_p \simeq 1\,000\,\text{K kg}^{-1}$, $\bar{T}_s \simeq 730\,\text{K}$ and $F_s \simeq 100\,\text{W m}^{-2}$. The determination of the internal structure parameters is by far, the most complicated. For the core radius we choose $R_c \sim 3.2 \times 10^6$m (Yoder, 1995b) and for the mantle elastic deformation correction we use the Earth value $\gamma_{el} \sim 0.75$ (Sasao *et al.*, 1980). The total polar moment of inertia, C, and the polar moment of inertia of the core, C_c, fall within (Yoder, 1997):

$$0.331 \leq \frac{C}{mR^2} \leq 0.341 \; ; \quad 0.020 \leq \frac{C_c}{mR^2} \leq 0.041 \; ; \quad (1)$$

In our simulations we used $(B - A)/C = 2.16 \times 10^{-6}$ (Konopliv *et al.*, 1993), $C/mR^2 = 0.336$, and $C_c/C = 0.084$, the same values as Yoder (1995a, 1997). All the other dissipative parameters appearing in the equations of (V2) are submitted to large uncertainties, namely, the tidal phase lags $\delta^\tau(\sigma)$, the effective viscosity ν and the non-hydrostatic core ellipticity δE_c. In the standard model, that we will use as a reference, these parameters are chosen as the most probable for our present understanding of the internal structure of terrestrial planets.

2.1.1 Gravitational tides model

The choice of a tidal dissipation model to Venus is not easy. Venus is believed to spin rapidly at the beginning of its evolution which contrasts with the present slow rotation. For slow rotation rates ($\omega \sim n$), a viscous model is the most appropriate, while for fast rotation rates, the best choice seems to be the constant Q model (see V2). Therefore, we have decided to use an interpolated model which behaves like the viscous one for small tidal frequencies ($\sigma \sim n$), but that resumes to the constant one for high tidal frequencies ($\omega \gg n$). The interpolation function between those two models is then (V2, Eq.29):

$$b^g(\sigma) = \text{sign}(\sigma)\frac{k_2}{Q_f}\left(1 - (1 - Q_f/Q_n)^{\frac{|\sigma|}{n}}\right) \; , \quad (2)$$

where Q_f is the quality factor for the fast rotating planet and Q_n the same factor but for $\sigma = n$. The relation between the quality factor and the phase lag is (V2, Eq.25):

$$Q_\sigma \simeq \frac{1}{2\delta^g(\sigma)} = \frac{1}{\sigma\Delta t^g(\sigma)} \; . \quad (3)$$

The Q factor for planets and satellites in the Solar System was estimated to be within (Goldreich and Soter,

1966):

$$10 < Q < 500 \; . \quad (4)$$

In the particular case of Q_n we know that the inferior limit is raised to $Q_n > 45$ in order to maintain the present observed equilibrium between gravitational and atmospheric tides (V2, Eq.96). In addition, for a given initial rotation rate ω_i, the time Δt_f needed to attain the present spin state is given by (V2, Eq.105) :

$$\Delta t_f \propto Q\omega_i \; . \quad (5)$$

Hence, it is not possible to choose much higher values than 45 for Q_n as this will not allow to decelerate the spin rate to the present value within the age of the Solar System. Thus, as Yoder (1995a, 1997), we set $Q_n = 50$ in the standard model. Some authors defend that in the first billion years, planets should dissipate more energy (eg. Burns, 1976, Lambeck, 1980, Dobrovolskis, 1980). In the case of Venus this also coincides with the period of fast rotation, so $10 < Q_f < Q_n$. In (V1) we used $Q_f \simeq 21.5$, the Earth's present observed value (with $\sigma = 2\pi$ d^{-1}), derived from the laser measures of the Earth-Moon distance (Dickey *et al.*, 1994). However, this is a lower limit, as for the present Earth, the main dissipation is supposed to come from the oceans (see Lambeck, 1988). Even though Venus could have had an ocean in the past, we will choose here for the standard model a value of Q_f twice larger than the Earth one, i.e., $Q_f = 40$.

2.1.2 Atmosphere model

The adopted model for the thermal atmospheric tides is described in detail in (V2). We use for ground pressure variations $\delta\tilde{p}(\sigma)$ a smoothed heating at the ground model (Dobrovolskis and Ingersoll, 1980):

$$|\delta\tilde{p}(\sigma)| = \frac{5}{16}\frac{\gamma}{|\sigma|}\frac{gF_s}{c_p\bar{T}_s}\left(1 - e^{-10^3\left(\frac{2\sigma}{n}\right)^2}\right) \; , \quad (6)$$

and we suppose that the ratio between the dissipation time lags of the gravitational and the atmospheric tides is constant and equal to its present value, i.e. (V2, Eq.100),

$$\frac{\Delta t^a(\sigma)}{\Delta t^g(\sigma)} \simeq \frac{\Delta t^a(2\omega_s)}{\Delta t^g(2\omega_s)} \simeq 36.5 \; . \quad (7)$$

This assumption implies that we are using for atmospheric tides, the same dissipative model as for gravitational tides (an interpolated model in this case). The arguments used to support this choice are the same that justified it for gravitational tides (different behaviors for fast and slow rotation rates). However, this model has a crucial improvement comparing with previous studies, as in this case, the ratio $\Delta t^a(\sigma)/\Delta t^g(\sigma)$ tends to the present observed value for $d\omega/dt = 0$.

Another source of uncertainty is the evolution of the atmosphere. In fact, it is largely accepted that terrestrial

planets' dense atmospheres are supposed to be secondary atmospheres that result from a degassing process over several hundred million years (Walker, 1975, Hart, 1978, Melton and Giardini, 1982, Zahnle *et al.*, 1988, Hunten, 1993, Pepin, 1991, 1994). According to current scenarios, in the early stages of the planet, there was an extreme ultraviolet radiation from the young evolving Sun, a few hundred times above the levels of the present values (eg. Walter and Barry, 1991), that was responsible for the loss of the hydrogen-rich primordial atmospheres. The generated hydrogen escape flux was large enough to exert upward drag forces on heavier atmospheric constituents, sufficient to lift them out of the atmosphere (blowoff). This process is assumed to last at least 300 Ma (Pepin, 1991, Hunten, 1993). More, the impact of a planetesimal can erode part or the totality of the existing atmosphere or add volatiles to it. The competition between accretion and erosion depends on the composition of the impactor and on the mass of the growing planet (Melosh and Vickery, 1989, Hunten, 1993). Thus, since the "heavy bombardment" was probably not finished before 800 Ma (Chyba, 1987, Kasting, 1993), it is commonly assumed that the secondary atmosphere only comes out after this date. Finally, the past strength of the semiannual tide is also affected by the transparency history of the Venusian atmosphere. Presently, only 100 out of $2\,600\,\mathrm{W\,m^{-2}}$ reach the surface (Avduevskii *et al.*, 1976). If the solar flux absorbed by the ground F_s, were larger in the past such that the mean surface temperature were higher, then the thermal atmospheric tides could be smaller. On the contrary, if the greenhouse mechanism were less effective the mean surface temperature could be lower, and atmospheric tides could be larger.

For all these reasons, we will not consider the effect of the atmosphere from the very beginning of the Solar System. In our standard model the accretion of the atmosphere will only start after 300 Ma (blowoff) and the surface pressure will grow linearly up to 800 Ma (end of the heavy bombardment). This will be quantified by a weight function $\zeta(t)$, which gives the ratio of the surface pressure variations of the date (t) over the present ones, as:

$$
\zeta(t) = \left\{
\begin{array}{ccc}
0 & \text{if} & t \leq 0.3\,\mathrm{Ga} \\
(t_{\mathrm{Ga}} - 0.3)/0.5 & \text{if} & 0.3\,\mathrm{Ga} < t < 0.8\,\mathrm{Ga} \\
1 & \text{if} & t \geq 0.8\,\mathrm{Ga}
\end{array}
\right.
\tag{8}
$$

2.1.3   Core-mantle friction model

The general theory of the secular variations of the spin due to the core-mantle friction (CMF) inside the planet is described by Rochester (1976). The dynamical equations depend on a coupling parameter κ that is not known for Venus, and even for the Earth, we do not have at present

a solid estimation. Indeed, κ is proportional to the square root of the cinematic viscosity ν (Roberts and Stewartson, 1965, Busse, 1968) whose uncertainty covers about 13 orders of magnitude (Lumb and Aldridge, 1991). It can be as small as $\nu = 10^{-7}\,\mathrm{m^2\,s^{-1}}$ for the Maxwellian relaxation time and experimental values for liquid metals, or as big as $\nu = 10^5\,\mathrm{m^2\,s^{-1}}$ for the damping of the Chandler wobble or attenuation of shear waves. The best estimate so far of the actual value of this parameter is $\nu \simeq 10^{-6}\mathrm{m^2s^{-1}}$ (Gans, 1972, Poirier, 1988). As in some previous studies on the Venus spin dynamics, we will then use this value in the standard model.

In addition, unlike the Earth's case, friction between the core and the mantle on Venus may become turbulent. In fact, for slow rotation rates, the Reynolds' number (Re) for precessional flow is so large that turbulence at the core-mantle boundary is almost certain unless the angle between the core and the mantle spin vectors is extremely small (see V2). Turbulence usually sets in for Re $\sim 10^5$ to 10^6. To delay the onset of the turbulence, we will chose $\mathrm{R}_T = 10^6$. We then compute $u_D/u_0 \simeq 1/13.87$ to ensure the continuity between the two regimes. Once in the turbulent regime, the CMF does not depend anymore on the viscosity. However, this will not simplify the motion equations, as for slow rotation rates, the non-hydrostatic term of the core ellipticity δE_c, which is also unknown, becomes dominant. This parameter depends on the irregularities of the core-mantle boundary, which can reach several kilometers (Hide, 1969). Yoder (1995a) computes a theoretical value for the non-hydrostatic core ellipticity, $\delta E_c \simeq 29\delta E_d$, but he recognizes that it is probably too large (though not physically unreasonable). We prefer here to assume the Venusian ellipticity to be closer to the Earth one, with estimated value $\delta E_c \simeq 4\delta E_d$ (Herring *et al.*, 1986).

2.2   Simulations excluding planetary perturbations

Having chosen a dissipation model for the long term evolution of Venus' spin, we can now perform numerical simulations. Before looking at the global dynamic of the spin, we have integrated first the equations without planetary perturbations. There are two main reasons for this choice: The first one is historical. Before the discovery of the importance of the chaotic zone for the obliquity (Laskar and Robutel, 1993), all the studies on the subject excluded this effect (Lago and Cazenave, 1979, Dobrovolskis, 1980, Shen and Zhang, 1989, McCue and Dormand, 1993, Yoder, 1995a). Thus, it is easier to compare the results of the standard model with ancient models when planetary perturbations are not taken into account. Furthermore, the scenarios where planetary perturbations were considered (Néron de Surgy, 1996, Yoder, 1997, Correia and

Laskar, 2001) also analyzed the non perturbed behavior. The other reason why we do not want integrate the global equations immediately is to enhance the importance of the effect of chaotic zone on the final evolution of Venus.

2.2.1 A first numerical experiment

In Fig. 1 we have traced different evolutions of the Venusian obliquity for an initial rotation period $\mathcal{P}_i = 3$ d (initial rotation rate $\omega_i \simeq 75n$). As expected (Tab. 1), the final obliquity is either $0°$ or $180°$. For initial obliquity values higher than the critical obliquity of $\varepsilon_i = 31.4°$, the planet's axis is always tilted to $180°$ and the rotation is decelerated till the final period $\mathcal{P}_f = 243.02$ d ($\omega_f = 0.92\,n$). This corresponds to the final state $\mathcal{F}_\pi^-$ (Table 1), a retrograde rotation state which is in agreement with the present observed situation of Venus. On the contrary, for initial obliquities lower than $\varepsilon_i = 31.4°$ the planet's axis is straightened to $0°$. However, we must differentiate here between two possible evolutions: the most common one, when $\varepsilon_i < 25.4°$, where the rotation is decelerated till $\mathcal{P}_f = 76.83$ d ($\omega_f = 2.92\,n$). This corresponds to the direct rotation final state $\mathcal{F}_0^+$ (Table 1). The other possibility is obtained when the initial obliquity lies between $25.4°$ and $31.5°$. Here, the rotation rate brakes till zero and thereafter accelerates in the reverse direction, the stabilization occurring in the final state $\mathcal{F}_0^-$ (Table 1), where $\mathcal{P}_f = -243.02$ d ($\omega_f = -0.92\,n$). This corresponds to a scenario which was suggested by Kundt (1977), although without analytical arguments.

state	ε	ω	$\mathcal{P}$ (days)
$\mathcal{F}_0^+$	$0°$	$n + \omega_s$	76.83
$\mathcal{F}_0^-$	$0°$	$n - \omega_s$	-243.02
$\mathcal{F}_\pi^+$	$180°$	$-n - \omega_s$	-76.83
$\mathcal{F}_\pi^-$	$180°$	$-n + \omega_s$	243.02

Table 1: **Possible final spin states of Venus, in absence of planetary perturbations (Correia and Laskar, 2001).** There are two retrograde states ($\mathcal{F}_0^-$ and $\mathcal{F}_\pi^-$) and two direct states ($\mathcal{F}_0^+$ and $\mathcal{F}_\pi^+$).

2.2.2 Critical points and final states

The different scenarios described in the previous section are easy to understand with the help of Fig. 2, where the rotation rate ($\dot{\omega}$) is plotted versus (ω), for a fixed obliquity value at $\varepsilon = 0°$ (a) and $\varepsilon = 180°$ (b). In these graphics, the final evolution of Venus corresponds to one of the three critical fixed points ($\dot{\omega} = 0$). As the central fixed point ($\mathcal{I}_0$ or $\mathcal{I}_\pi$) is unstable, the only possible final evolutions are the four stable critical points corresponding to $\mathcal{F}_0^-, \mathcal{F}_0^+, \mathcal{F}_\pi^-, \mathcal{F}_\pi^+$. As we assume that at the origin $\omega > 0$ (this is not a restriction, as retrograde initial rotations are
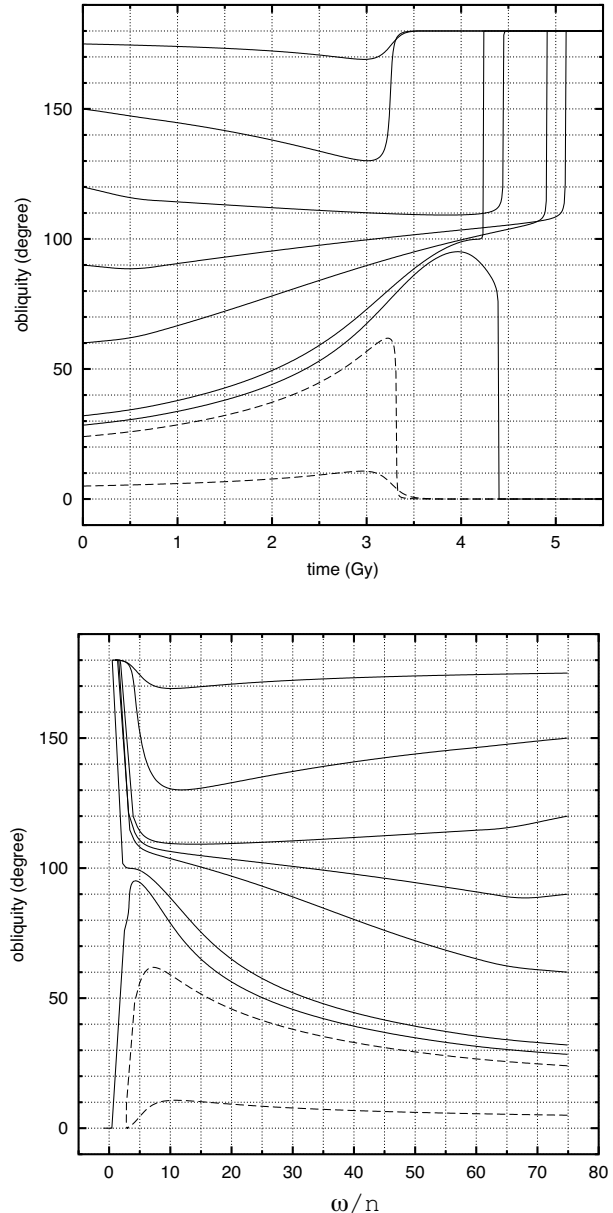

Figure 1: **Obliquity evolution in time (a) and with respect to the rotation rate (b) using the standard model.** Since we start our integrations with $\omega_i \simeq 75\,n$ ($\mathcal{P}_i = 3$ d), Fig. (b) must be read from the right to the left. Dotted lines correspond to direct final states and filled lines to retrograde final states. The transition initial obliquity between the direct states and the retrograde ones is $\varepsilon_i = 25.4°$ and $\varepsilon_i = 31.4°$ between the two retrograde states.

obtained with $\varepsilon > 90°$), Venus brakes from fast rotations so we always come from the right hand side of Fig. 2.

The final state where the planet will end depends on the value reached by ω when the obliquity comes close to $\varepsilon = 0°$ or $\varepsilon = 180°$. If $\omega > n$ when the obliquity ε approaches $0°$, the planet will tend towards the final state $\mathcal{F}_0^+$. On the contrary, if $\omega < n$ the spin will evolve to the
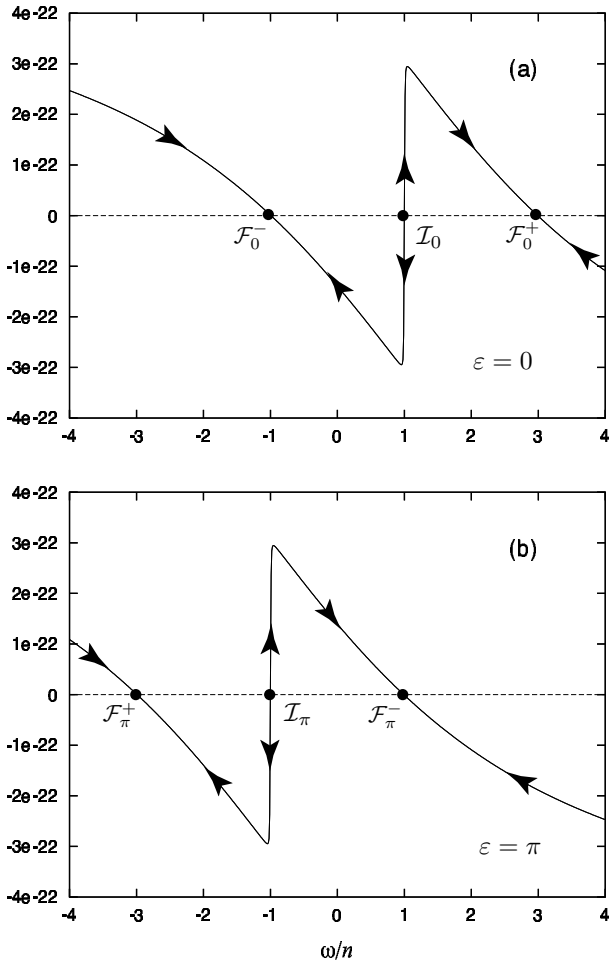
Figure 2: **Variation of $d\omega/dt$ upon ω/n considering all dissipative effects together at $\varepsilon = 0°$ (a) and $\varepsilon = 180°$ (b) (Correia et al., 2002).** As the central fixed point ($\mathcal{I}_0$ or $\mathcal{I}_\pi$) is unstable, the only possible final evolutions are the four stable points corresponding to $\mathcal{F}_0^+$, $\mathcal{F}_0^-$, $\mathcal{F}_\pi^+$ and $\mathcal{F}_\pi^-$.

retrograde final state $\mathcal{F}_0^-$. When the obliquity is brought to $0°$ during the first stages of the evolution, the rotation rate will not be much reduced and will always verify $\omega > n$. It will then be impossible to reach the retrograde final state $\mathcal{F}_0^-$. However, if the obliquity is far from $0°$ when the planet enters the slow rotation regime, the presence of the CMF effect allows the rotation rate to be reduced to values $\omega < n$ and the planet will evolve into the final state $\mathcal{F}_0^-$. When the obliquity evolves towards $180°$, dissipative effects always impose $\omega \geq -n$. The planet spin is then always on the right side of $\mathcal{I}_\pi$, and the only possibility is to finish in the final state $\mathcal{F}_\pi^-$.

2.2.3 Numerical simulations and the $\mathcal{F}_0^-$ state.

Figure 3 is similar to Fig. 1b, but with initial obliquities $\varepsilon_i = 25°, 26°$, and $\varepsilon_i = 31°, 32°$, which are bracketing the critical initial obliquities ($\varepsilon_i = 25.4°$ and $\varepsilon_i = 31.4°$). Only the final part of the evolutions are displayed in order to differentiate more clearly the behavior near these critical obliquities. The evolution into the direct final state $\mathcal{F}_0^+$ or into the retrograde state $\mathcal{F}_0^-$ will depend whether the CMF reduces the rotation rate ω to a value superior to n or not as shown in Fig. 2a. The evolution into each retrograde final state depends whether the obliquity is above (final state $\mathcal{F}_\pi^-$) or below $90°$ (final state $\mathcal{F}_0^-$), when the CMF effect becomes dominant.
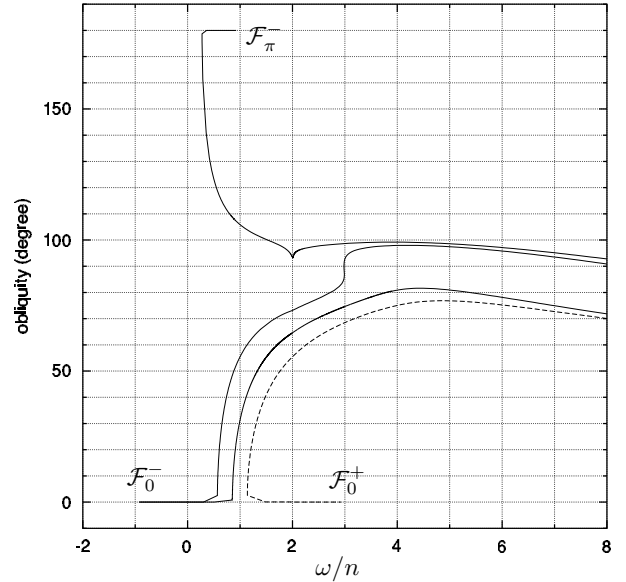

Figure 3: **Final evolution of Venus' obliquity versus rotation rate for the initial obliquity values: $\varepsilon_i = 25°$, $26°$ and $\varepsilon_i = 31°$, $32°$ (standard model).** The difference between the evolution into the direct final state $\mathcal{F}_0^+$ and the evolution into the retrograde state $\mathcal{F}_0^-$ depends whether the CMF effect reduces the rotation rate ω to a value superior to n (direct final state) or inferior to n (retrograde final state) as shown in Fig. 2a. The difference between the evolution into each retrograde final state depends on whether the obliquity is above $90°$ (final state $\mathcal{F}_\pi^-$) or below $90°$ (final state $\mathcal{F}_0^-$) when the CMF effect become dominant.

The zone of retrograde states $\mathcal{F}_0^-$ which appears within the two critical obliquities was not observed in previous studies (Lago and Cazenave, 1979, Dobrovolskis, 1980, Shen and Zhang, 1989, McCue and Dormand, 1993, Yoder, 1995a, 1997, Néron de Surgy, 1996) because of their choice of atmospheric tides models (see V2, section 3.1.2) which introduced an infinite singularity at $\omega = n$.

2.2.4 The initial spin rate of Venus.

The initial spin rate of Venus is not known as very little constraint can be derived from the present planetary formation models. A small number of large impacts at the end of the formation process of a planet will not average, and can change its spin rate or direction (Dones and
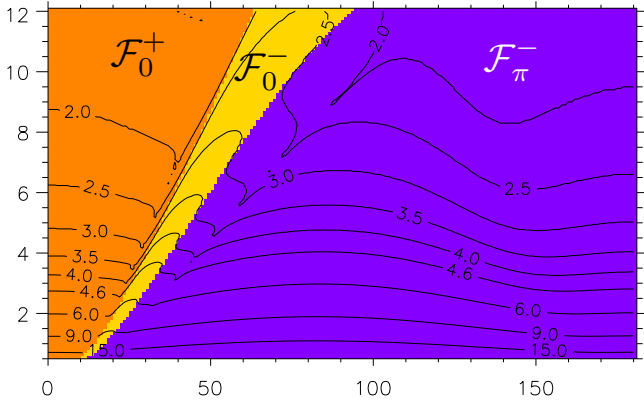
Figure 4: **Final states of Venus' spin for initial obliquity ($\varepsilon_i \in [0°, 180°]$) and period ($\mathcal{P}_i \in [0.5\,\text{d}, 12\,\text{d}]$) in absence of planetary perturbations.** Initial periods are comprised between 0.5 days (12 hours) and 12 days with a step size of 0.1 day and starting with any obliquity (from 0° to 180°) with an increment of 1°. We can distinguish three final evolutions. The larger one (dark grey) corresponds to the retrograde final state $\mathcal{F}_\pi^-$, that occurs for high initial obliquities. For small initial obliquities the planet always evolves to the direct final state $\mathcal{F}_0^+$ (grey). Between these two possibilities, we find the zone of the retrograde final state $\mathcal{F}_0^-$ (light grey). The time after which the final state is reached is indicated by curved labeled in Ga.

Tremaine, 1993), and on the other hand, the empirical relation $\omega_i = K m^{4/5} R^{-2}$ given by MacDonald (1964) leads to $\mathcal{P}_i \simeq 13.5$ hours for Venus. Overall, the only strong constraint on the initial spin rate of Venus seems to be its present observed slow rotation.

In Figs. 1 and 3, we chose for the initial rotation period $\mathcal{P}_i = 3$ days as it is the fastest initial period that allows almost any initial obliquity to evolve into a final states within the age of the Solar System. Evolutions with slower initial rotation periods can be easily depicted from Fig. 1b choosing a slower initial rotation rate as starting point and ignoring the previous evolution. If we assume a stronger dissipation, i.e., a smaller value of Q, we can set the initial rotation rate ω_i to higher values, as $\omega_i \propto Q^{-1} \Delta t_f$, where Δt_f is the time required to reach a final state (Eq.5).

In order to cover all possible scenarios for the initial spin of Venus, we have computed the possible evolutions for a planet starting with an initial period comprised between 0.5 days (12 hours) and 12 days, with a step size of 0.1 day and starting with any obliquity (from 0° to 180°) with an increment of 1°. Results are plotted in Fig. 4 where each color represents a final state, and the numbered level curves give the time in Ga needed to reach this state. We can distinguish here only three final evolutions (the direct states $\mathcal{F}_\pi^+$ are not reachable). The larger one (dark grey) corresponds to the retrograde final state $\mathcal{F}_\pi^-$, that occurs for high initial obliquities. For small initial obliquities the planet always evolves to the direct final state $\mathcal{F}_0^+$ (grey). Between these two possibilities, we find the zone of the

retrograde final state $\mathcal{F}_0^-$ (light grey). The separating curves between each final evolution are, in this case, more or less straight lines which relates the initial period (in days) to the initial obliquity (in degrees), as

$$\mathcal{P}_i^- = 0.14\,\varepsilon_i - 1.6 \; ; \quad \mathcal{P}_i^+ = 0.24\,\varepsilon_i - 3.4 \; . \quad (9)$$

Using the results plotted in Fig. 4, we tested expression (5) for a constant Q value. For each initial obliquity we plotted the initial rotation rate ω_i versus the time Δt_f needed to reach a final state ($|\omega - \omega_f|/n < 10^{-5}$) (Fig. 5). We obtain roughly linear relations, in agreement with (5), except for initial obliquities that intersect different final states.

2.3 Effect of planetary perturbations

The planetary perturbations are now introduced using the full secular system for the motion of the whole Solar System (Laskar, 1990, 1994). This allows to have a good model for planetary perturbations, with reasonable CPU time, despite the fact that we will perform the integrations over several billion years. As the Solar System motion is chaotic, we do not expect that the computed solution will correspond to the precise evolution of the planets. However, since the diffusion of the trajectories is moderated (Laskar, 1994), we assume that this solution will be representative of the true planetary perturbations.

2.3.1 Final states with planetary perturbations

When planetary perturbations are considered, an important modification occurs with the four final states characterized in table 1. As explained in section 4.5 of (V2), due to the forced obliquity $\delta\varepsilon$, the final rotation rates ω_f will no longer correspond to steady states, because the obliquity variations give rise to a variation $\delta\omega$ (V2, Eq.110):

$$|\delta\omega| = n\varrho(n/|\omega_f|)^{5/2}\delta\varepsilon^2 \; , \quad (10)$$

where ϱ is a measure of the strength of the CMF and tidal effects. The range of $\delta\omega$ depends on the "mean" final rotation rate ω_f and on the range of forced obliquity variations, obtained numerically.

For the retrograde rotation final states, we can still use the present observed rotation period as the "mean" rotation period of those final states. However, as it is shown by (V2, Eq.111), for the direct rotation final states, the rotation periods given in table 1 are no longer valid. Indeed, for those final states, the precession constant ($\alpha \simeq 14.7"/\text{yr}$) lies near the chaotic zone and thus, the forced obliquity variations will be larger. Numerical experiments (using the standard model) show that for the retrograde final states, the forced obliquity has a maximum amplitude of 2°, whereas for the direct final states it can be as large as 8°. According to expression (V2,
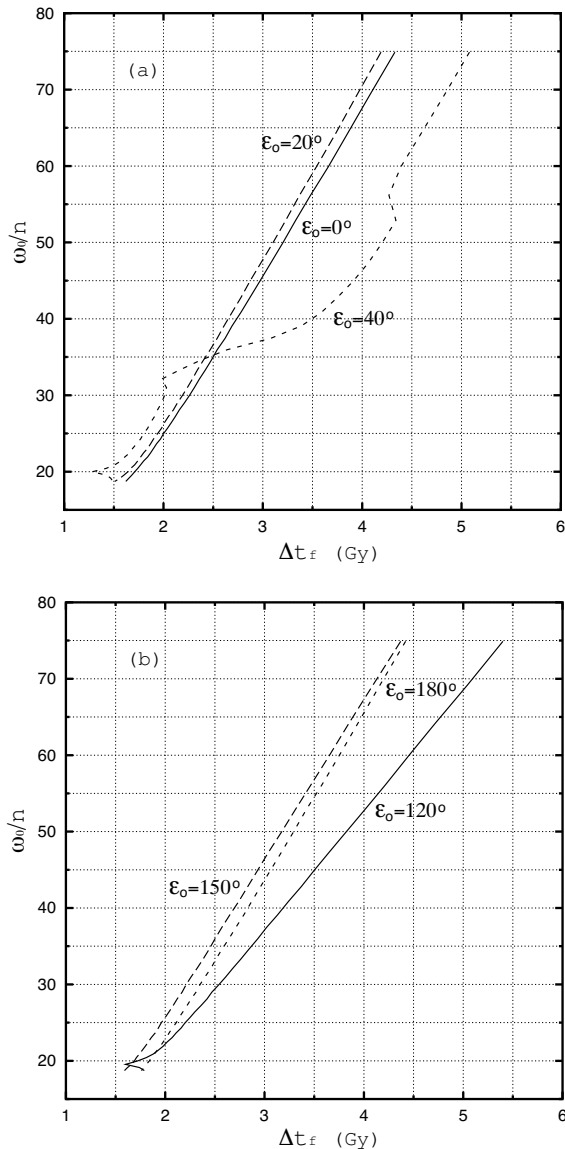
6

state	$\overline{\varepsilon}$	$\delta\varepsilon_{\max}$	$\overline{\mathcal{P}}$ (days)	$\Delta\mathcal{P}$ (days)
$\mathcal{F}_0^+$	$5°$	$8°$	135	± 5
$\mathcal{F}_0^-$	$1°$	$2°$	-243	± 1
$\mathcal{F}_\pi^+$	$175°$	$8°$	-135	± 5
$\mathcal{F}_\pi^-$	$179°$	$2°$	243	± 1

Table 2: **Possible final spin states of Venus, in presence of planetary perturbations.** There are two retrograde states ($\mathcal{F}_0^-$ and $\mathcal{F}_\pi^-$) and two direct states ($\mathcal{F}_0^+$ and $\mathcal{F}_\pi^+$), but the rotation final periods are no longer completely steady.

Figure 5: **Initial rotation rate ω_i versus the time needed to reach a final state Δt_f, for $\varepsilon_i = 0°$, $20°$ and $40°$ (a) and for $\varepsilon_i = 80°$, $150°$ and $180°$ (b) using the standard model.** For a constant value of Q we see that expression (5) is verified for any obliquity, except when occurs a transition from one final state to another.

Eq.112), the rotation period of the direct rotation final states will then be increased, which is confirmed in our numerical experiments, where we observe that the final rotation period is within 130 and 140 days. The new mean periods are given in table 2 (to be compared with table 1).

In his study of Venus' free obliquity, Yoder (1995a) find numerically for the retrograde final states obliquity variations a "mean" obliquity of about $2°$, while for some sets of the dissipation parameters, the maximal obliquity can reach up to $4°$. The difference with our values results from

two main reasons: First, while Yoder uses a constant Q model, our model is linear for slow rotation rates. The second difference is that Yoder takes into account the actual separation of about $0.5°$ between the axis of rotation and the axis of greatest inertia. As explained in (V2), we have merged these two axis for our long-term integrations.

2.3.2 Standard model with $\mathcal{P}_i = 3\,\mathrm{d}$ and $\varepsilon_i = 1°$

As the chaotic dynamics prevents one or few integrations to be representative of the possible past evolution, we have performed exhaustive numerical experiments. Setting the initial rotation period to $\mathcal{P}_i = 3$ d and the initial obliquity to $\varepsilon_i = 1°$ we have simultaneously integrated over 4.6 Ga, 100 orbits with initial precession angles separated by 0.05 rad. We will not plot of course all these trajectories, but only a selection of them, corresponding to some typical behavior. With these settings, we obtained the three different final evolution states, $\mathcal{F}_0^+$, $\mathcal{F}_0^-$ and $\mathcal{F}_\pi^-$ (Fig. 8a-c). In absence of planetary perturbations we have seen in the previous section that for any initial obliquity lower than $25.4°$ the planet always ended in the direct final state $\mathcal{F}_0^+$. However, the passage trough the chaotic zone now allows the obliquity to drift between $0°$ and almost $80°$, far beyond the $25°$ level, and only a part of the trajectories finishes in the direct rotation state. The other trajectories lead to one of the retrograde rotation final states $\mathcal{F}_0^-$ or $\mathcal{F}_\pi^-$. The paths which drive to each final state are quite different, and in Fig. 6, we have plotted the evolution of the maximal and minimal obliquity for all initial conditions leading to the same final state.

Since we started with $\mathcal{P}_i = 3$ d, the initial precession constant is $\alpha_0 = 16.2"/\mathrm{yr}$ (V2, Eq.2), which corresponds to the chaotic zone, but with moderated diffusion (Figs 9a-c). This is why the maximal obliquity increases from $1°$ to about $20°$. After 1 Ga, the maximal obliquity can reach $40°$. However, as soon as the precession constant decreases below $\alpha \simeq 10"/\mathrm{yr}$ ($\omega \sim 45n$), the planet will enter in the strong chaotic zone. Here, the maximal obliquity largely increases up to $70°$. Moreover, the amplitude of the obliquity variations can now sweep more than $50°$ in a few million years, as it is illustrated in Fig. 7. Due to dissipative effects, the precession constant decreases till $\alpha = 5.85"/\mathrm{yr}$
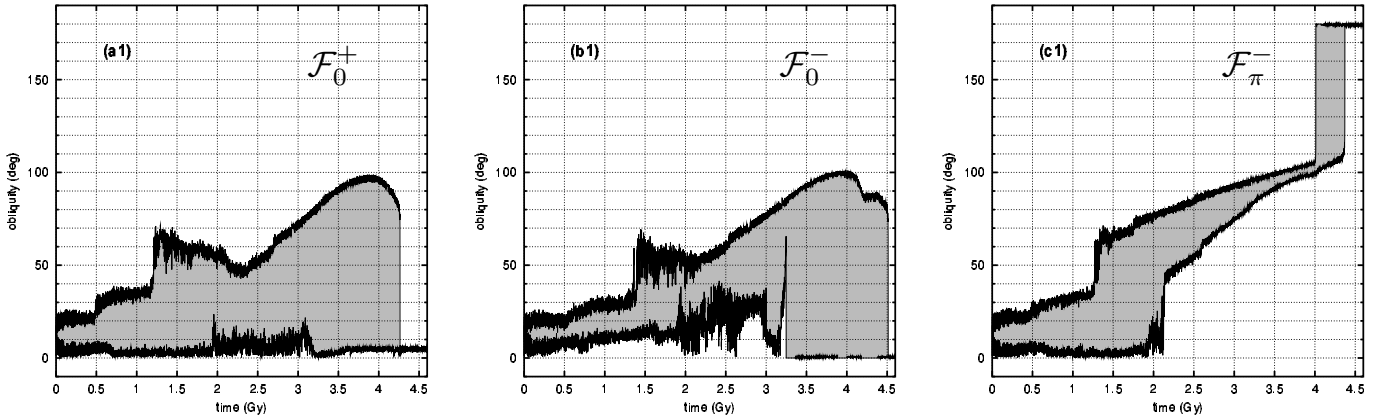
Figure 6: **Maximal and minimal obliquity evolution in time.** For the initial obliquity $\varepsilon_i = 1°$, we have simultaneously integrated 100 orbits with initial precession angles separated by 0.05 rad. Each image shows the maximal and minimal obliquities for all initial conditions leading to the same final state. The large augmentation in the maximal obliquity always present for ω comprised within $40n$ and $50n$ corresponds to the entry in the strong chaotic zone.
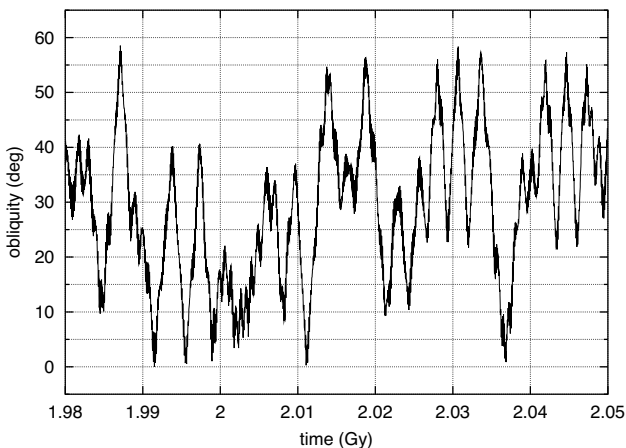

Figure 7: **Example of chaotic variation of the obliquity inside the chaotic zone.** When the precession constant of Venus is comprised within $5"/\mathrm{yr} < \alpha < 10"/\mathrm{yr}$, we can observe strong variations of the obliquity due to planetary perturbations, whose amplitude variations can reach $50°$ in a few million years.

$(\omega = 14n)$. Henceforth, its value increases again, because the non-hydrostatic term δE_d of the dynamical ellipticity E_d becomes dominant (V2). When α approaches its initial value $\alpha \sim 15"/\mathrm{yr}$ ($\omega \sim 3n$), the CMF effect becomes very strong and controls the spin evolution until the obliquity reaches near $0°$ or $180°$ values. During that time, the effects of planetary perturbations over the obliquity are unable to counteract the CMF dissipation.

2.3.3 Evolution with $\varepsilon_i = 60°$, $90°$ and $120°$

We have repeated the above study for initial obliquities $\varepsilon_i = 60°$, $90°$ and $120°$ (also in Figs. 8 and 9). In absence of planetary perturbations when we started with $\varepsilon_i = 60°$ the planet ended in the retrograde rotation final state $\mathcal{F}_\pi^-$ (Fig. 1b). Now, the planet can still evolve into this final state, but also to the retrograde rotation final state $\mathcal{F}_0^-$ or to the direct rotation final state $\mathcal{F}_0^+$. The reason is the same as for $\varepsilon_i = 1°$: the crossing of the chaotic zone allows the obliquity to decrease to low values and then to evolve eventually to another final state. However, as for $\varepsilon_i = 60°$ the planet starts deep inside the strong chaotic zone (Figs. 9d-f), strong obliquity variations can be observed from the very beginning.

When we set the initial obliquity at $90°$ (i.e., in the frontier between the chaotic and the stable zone), most of the trajectories evolve into the retrograde final state $\mathcal{F}_\pi^-$. Before the formation of the atmosphere, gravitational tides slightly decrease the initial obliquity (as shown in Fig. 1b), but this is not sufficient to bring it into the strong chaotic zone. However, the obliquity may encounter a resonance with the secular frequency of the Solar System s_8 (see section 2.6), where it has a small chance of being captured. In that case, the obliquity remains trapped below $90°$. When the CMF effect becomes very efficient, the planet leaves
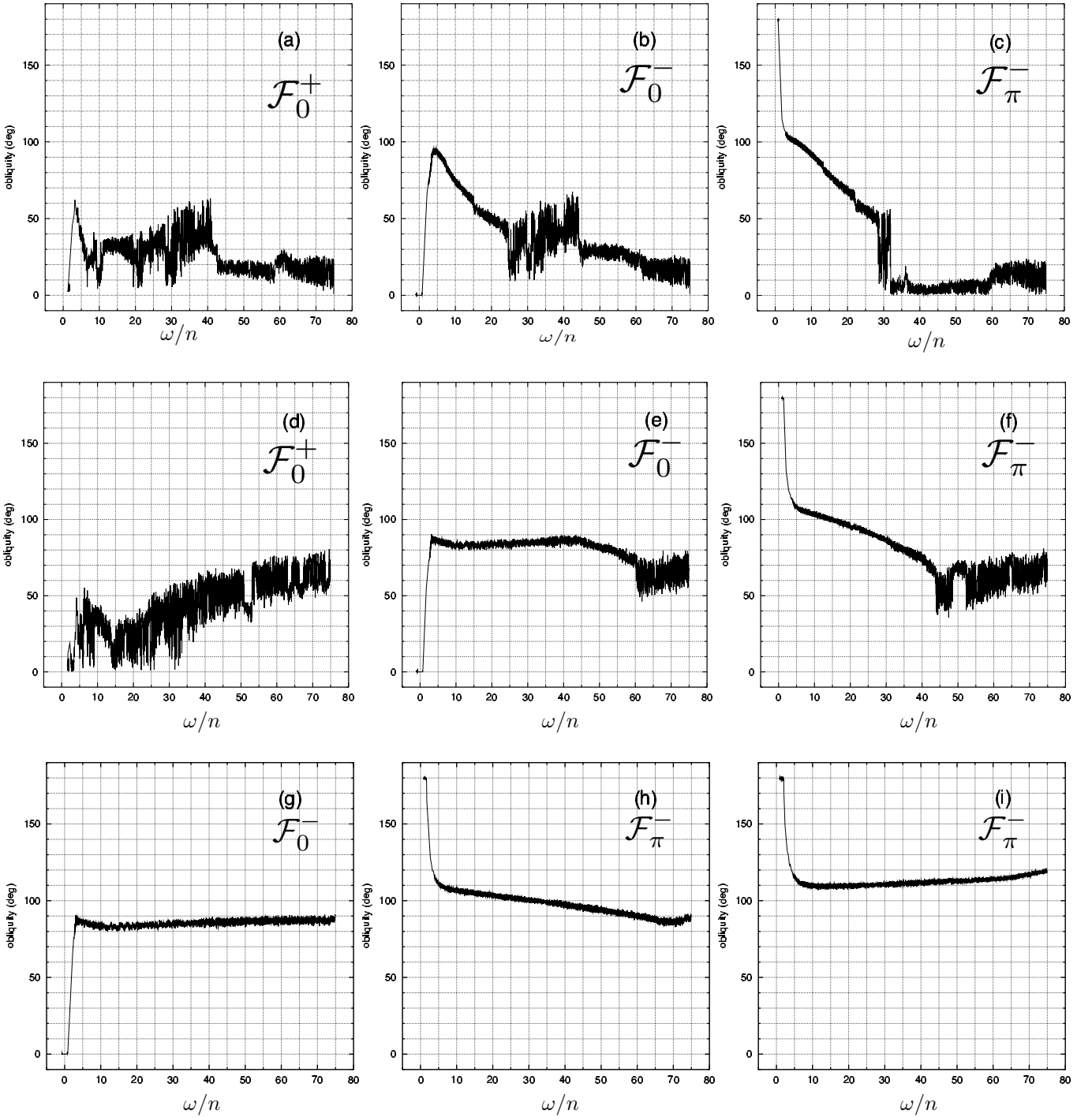
8

Figure 8: **Several examples of the possible evolution of the obliquity of Venus with the rotation rate, starting with $\mathcal{P}_i = 3$ d ($\omega \simeq 75n$).** Each evolution ends up in one of the three possible final rotation states: $\mathcal{F}_0^+$, $\mathcal{F}_0^-$ and $\mathcal{F}_\pi^-$. For $\varepsilon_i = 1°$ (a,b,c), the obliquity drifts between $0°$ and almost $80°$. The increase in the obliquity allows many trajectories to finish in one of the retrograde rotation final states $\mathcal{F}_0^-$ or $\mathcal{F}_\pi^-$, instead of the direct rotation state $\mathcal{F}_0^+$ as in the absence of planetary perturbations. Inversely, for $\varepsilon_i = 60°$ (d,e,f) the crossing of the chaotic zone can decrease the obliquity, allowing the planet to evolve into other possibilities than the final state $\mathcal{F}_\pi^-$. Finally, for $\varepsilon_i = 90°$ (g,h) and $\varepsilon_i = 120°$ (i), the only effect of the planetary perturbations is to add small oscillations of the obliquity around a mean value as we never cross the chaotic zone.
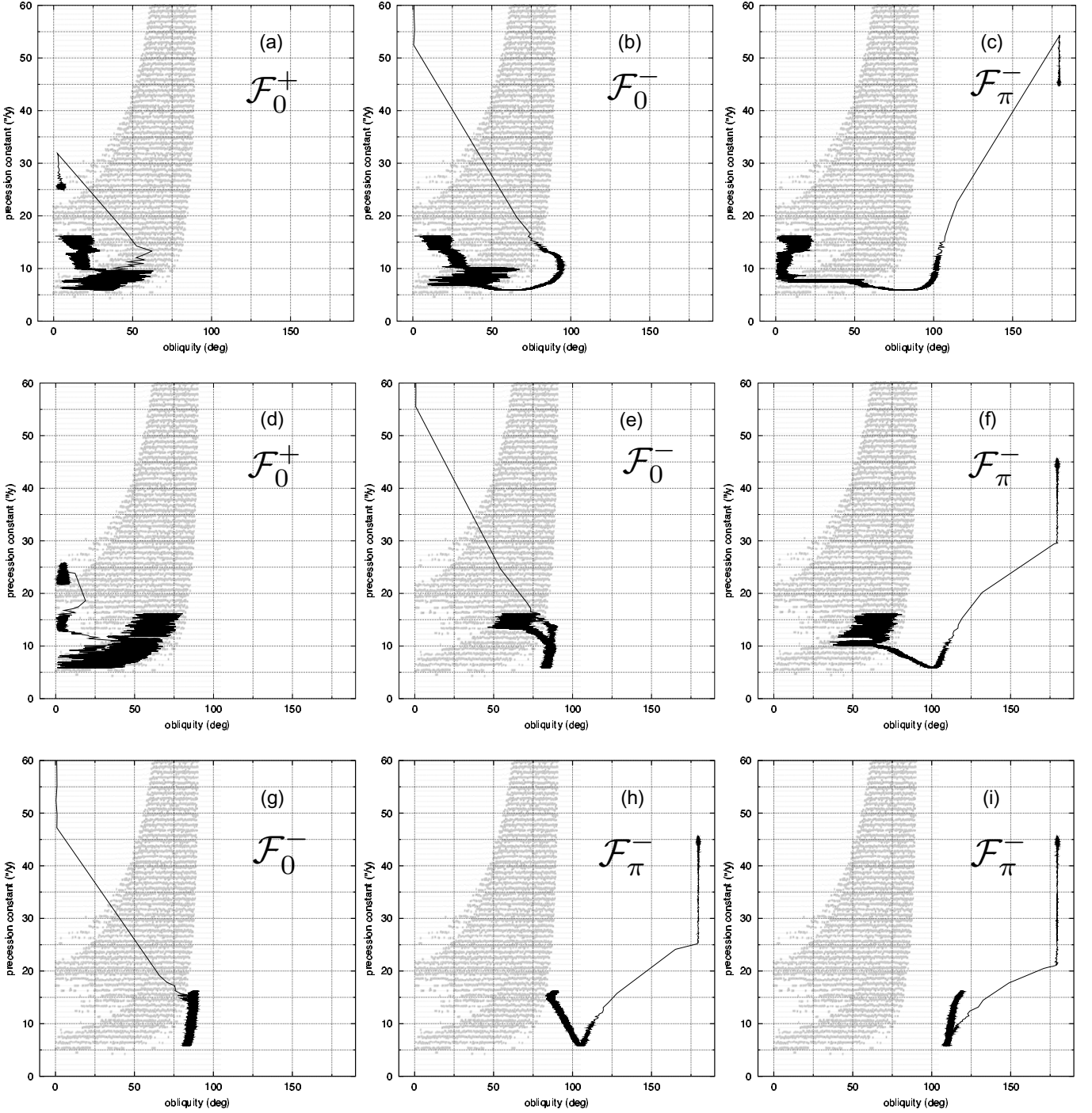
9

Figure 9: **Several examples of the possible evolution of the precession constant α with the obliquity, starting with $\alpha_0 =$ 16.2"/yr ($\mathcal{P}_i = 3$ d).** For $\varepsilon_i = 60°$ (d,e,f) the planet begins deep inside the chaotic zone, while for $\varepsilon_i = 1°$ (a,b,c) this zone is reached for $\alpha \sim 10$"/yr. There we can observe obliquity variations of about $50°$ in a few million years. For $\varepsilon_i = 90°$ (g,h) and $\varepsilon_i = 120°$ (i), the planet is outside the chaotic zone and we only observe small obliquity variations. Due to dissipative effects, the initial precession constant is slowly decreased until 5.85"/yr. Henceforth, it increases again, because the non-hydrostatic term δE_d of the dynamical ellipticity E_d becomes dominating. When the precession constant approaches again its initial value $\alpha \sim 15$"/yr, the CMF effect becomes stronger than planetary perturbations and it controls the entire evolution.

10

the resonance, and is driven into the direct final state $\mathcal{F}_0^+$ or to the retrograde final state $\mathcal{F}_0^-$, instead of the usual evolution towards $\mathcal{F}_\pi^-$ (Fig. 9g,h).

For $\varepsilon_i = 120°$ there is only one possible final evolution, which is the retrograde final state $\mathcal{F}_\pi^-$. In this case, independently of the precession initial phase, the different dynamical evolutions are very similar and they are close to the obliquity behavior in absence of planetary perturbations (Fig. 1b). This is quite understandable: since the entire evolution stays outside the chaotic zone, the only effects of the planetary perturbations is to add small oscillations to the unperturbed obliquity (Fig. 9i). The same behavior is expected for any evolution that never crosses the chaotic zone ($\varepsilon_i > 100°$).

2.4 Global view with planetary perturbations

In order to obtain a more global view, we have performed similar integrations as in Fig. 4, but with the addition of planetary perturbations. In Fig. 10 we show the possible final evolutions for a planet starting with an initial period ranging from 3 to 12 days, with an increment of 0.25 day, and initial obliquity from 0° to 180°, with an increment of 2.5 degrees (rotation periods faster than 3 days are excluded as they do not allow the planet to reach a final rotation state within the age of the Solar System). Each color represents one of the possible final states. As expected, for high initial obliquities, the final evolution of Venus remains essentially the same as without planetary perturbations since none of these trajectories encounters the chaotic zone. This is not the case for paths starting with low initial obliquities. Here, however, we can distinguish two different zones: one corresponding to slow initial rotation periods ($\mathcal{P}_i > 8$ d) where the direct rotation final state $\mathcal{F}_0^-$ is prevailing and another one for faster initial rotation periods, where we find a mixture of the three attainable final states, $\mathcal{F}_0^+$, $\mathcal{F}_0^-$ and $\mathcal{F}_\pi^-$.

For slow initial rotation periods, the initial precession constant is small, and the planet starts its evolution in the bottom of the chaotic zone (Fig. 9). The planet has thus less chances to increase its obliquity, as for slow initial rotation periods, the critical obliquities are higher (Eq.9). On the other hand, as the initial rotation period decreases, the critical obliquities have lower values, and the passage in the chaotic zone increases the probabilities of ending in a final state different than $\mathcal{F}_0^+$. This is why for fast initial rotation periods we find a random distribution of the three possible final states. To emphasize this chaotic behavior, we integrated this area twice more, with a difference of 10^{-9} in the initial eccentricity of Mars (Fig. 10b), and with a difference of 10^{-9} in the inital eccentricity of Neptune (Fig. 10c). Finally, in Fig. 11 we plotted several steps in the evolution of
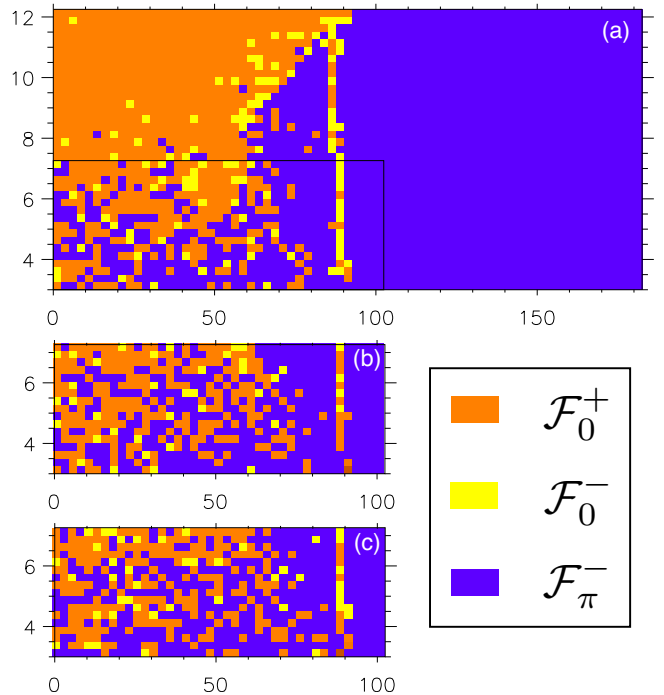

Figure 10: **Final states of Venus' spin for initial obliquity ($\varepsilon_i \in [0°, 180°]$) and period ($\mathcal{P}_i \in [3\,\text{d}, 12\,\text{d}]$) when planetary perturbations are included.** We have computed the possible evolutions for a planet starting with an initial period comprised between 3 and 12 days with a step size of 0.25 day and starting with any obliquity (from 0° to 180°) with an increment of 2.5°. For high initial obliquities, the final evolution of Venus remains essentially unchanged since none of these trajectories crossed the chaotic zone. The passage through this zone is reflected by the scattering of the final states in the left side of the picture. To emphasize the chaotic behavior in the bottom left corner of picture (a), we integrated it again with the same initial conditions, but with a difference of 10^{-9} in the initial eccentricity of Mars (b) and Neptune (c).

Venus, separated by 250 million years (with and without planetary perturbations), using the same technique as in Fig. 10. These sequences provide a global view of the evolution of the rotation period due to dissipative effects and planetary perturbations. The passage of each trajectory through the chaotic zone can be observed, as well as the time needed to reach a final state.

2.5 Final states probabilities.

The crossing of the chaotic zone, allows a trajectory to rapidly modify its obliquity and evolve to a final state that was not accessible in absence of planetary perturbations. The path in the chaotic zone is very sensitive to small changes in initial conditions or in the model, and it is thus impossible to preview in which final state it will end. However, this chaotic zone favors some trajectories, according to the initial conditions. In order to estimate
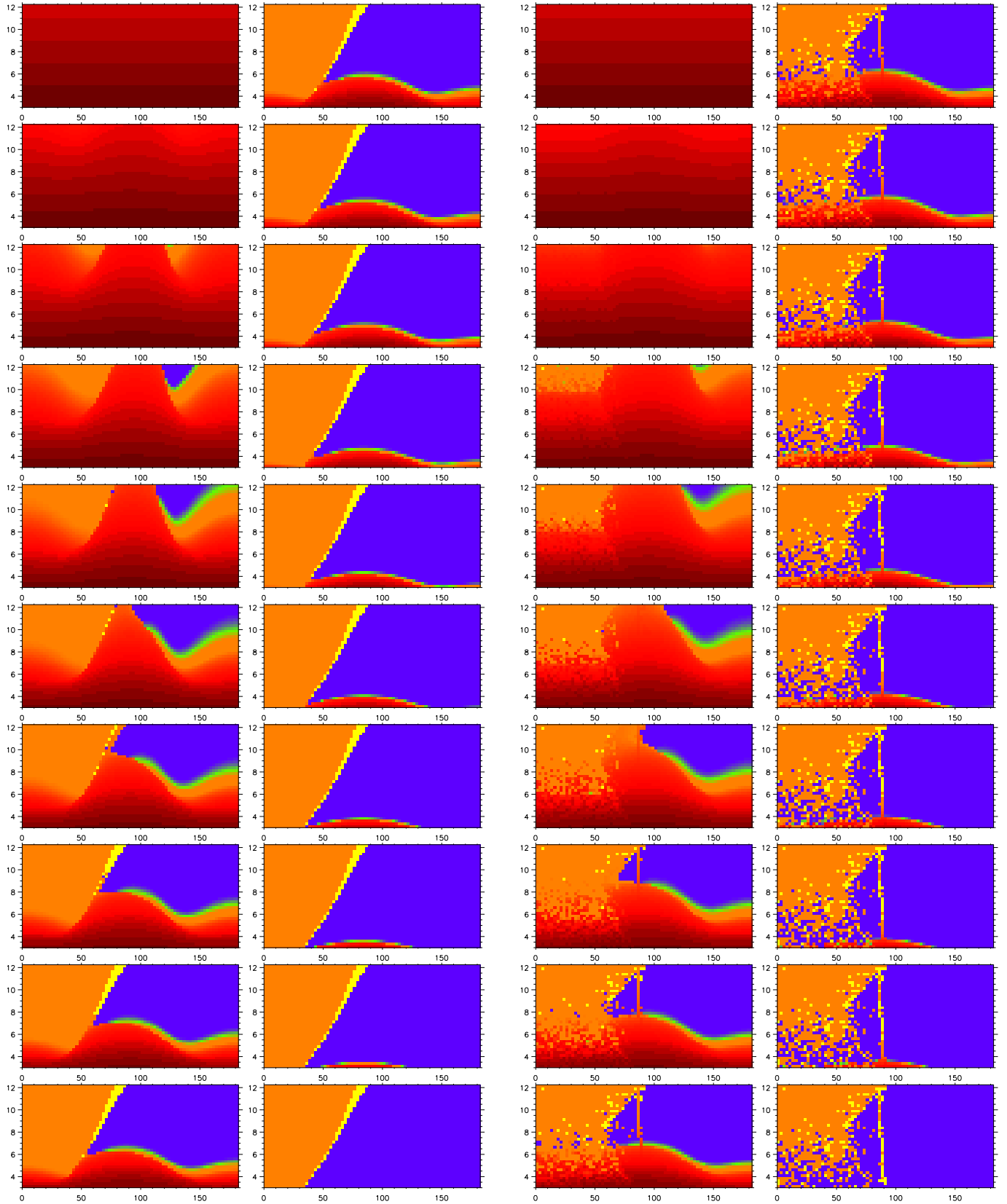
Figure 11: **Spin evolution of Venus.** Each picture is separated by 250 million years. Columns 1 and 2 correspond to a evolution without planetary perturbations, that are included in columns 3 and 4. This picture give us a global view of the modifications in time of the rotation period due to dissipative effects and due to planetary perturbations. The last figure of columns 2 and 4 correspond respectively to Fig. 4 and Fig. 10.

12

the probabilities of finishing in each final state, we have integrated the dynamical equations 100 times for every initial obliquity and initial periods of 3, 4, 5, 6, 7 and 8 days, changing between each initial condition the phase of the precession angle by 10^{-6} rad (Fig. 12).

Contrarily to the situation with no planetary perturbations (Fig. 4), the crossing of the chaotic zone allows any initial obliquity (with $\mathcal{P}_i < 8$ d) to evolve into the present observed state. For fast initial rotation periods or high initial obliquities, the retrograde final states are the most probable ones, but as the initial period increases, the direct final state $\mathcal{F}_0^+$ becomes dominant. For low obliquities ($\varepsilon_i < 60°$), the retrograde state $\mathcal{F}_0^-$ represents always about 10% of the possible final evolutions. For fast initial rotation periods, the $\mathcal{F}_0^-$ states represent less than 1/5 of all retrograde states, but for slow initial rotations, they become the majority of retrograde final states for low initial obliquities. This contrasts with the behavior described in section 2, where only initial obliquities comprised between 25° and 31° led to $\mathcal{F}_0^-$.

2.6 Secular resonances

In Fig. 10 we observe the presence of a narrow strip of initial conditions within $85° < \varepsilon_i < 90°$ that lead to the two final states $\mathcal{F}_0^+$ and $\mathcal{F}_0^-$ in a zone where the retrograde final state $\mathcal{F}_\pi^-$ is the most likely outcome. We will also see in sections 3, 4 that this strip is always present, independently of the dissipation models considered. Indeed, this curious effect results from the capture of the spin into a secular resonance with Neptune.

2.6.1 Resonance equations

The conservative Hamiltonian of the system with planetary perturbations writes (Laskar and Robutel, 1993):

$$\overline{\mathcal{H}} = \frac{L^2}{2C} - \alpha\frac{X^2}{2L} + 2\mathcal{C}(t)X$$
$$+ \sqrt{L^2 - X^2}\sum_{k=1} J_k \sin(\psi + \nu_k t + \phi_k) , \quad (11)$$

where ν_k are the secular frequencies of the orbital motion of Venus, J_k the amplitude of the perturbation and ϕ_k a phase angle. For an isolated frequency (ν_k), we retain only the k term in the Hamiltonian, and since $\dot{\psi} \simeq \alpha\cos\varepsilon$ (V2), expression (11) resumes to an integrable Hamiltonian similar to the one of a pendulum (Colombo, 1966, Ward, 1975, Henrard, 1987). Inside the resonance island, the obliquity will librate around the equilibrium value ε_e:

$$\cos\varepsilon_e = -\frac{\nu_k}{\alpha} , \quad (12)$$

and the maximal ε_+ and minimal ε_- obliquity values in the resonant island are given by:

$$\cos\varepsilon_\pm \simeq -\frac{\nu_k}{\alpha} \mp 2\sqrt{\frac{J_{\nu_k}}{\alpha}\sin\varepsilon_e} . \quad (13)$$
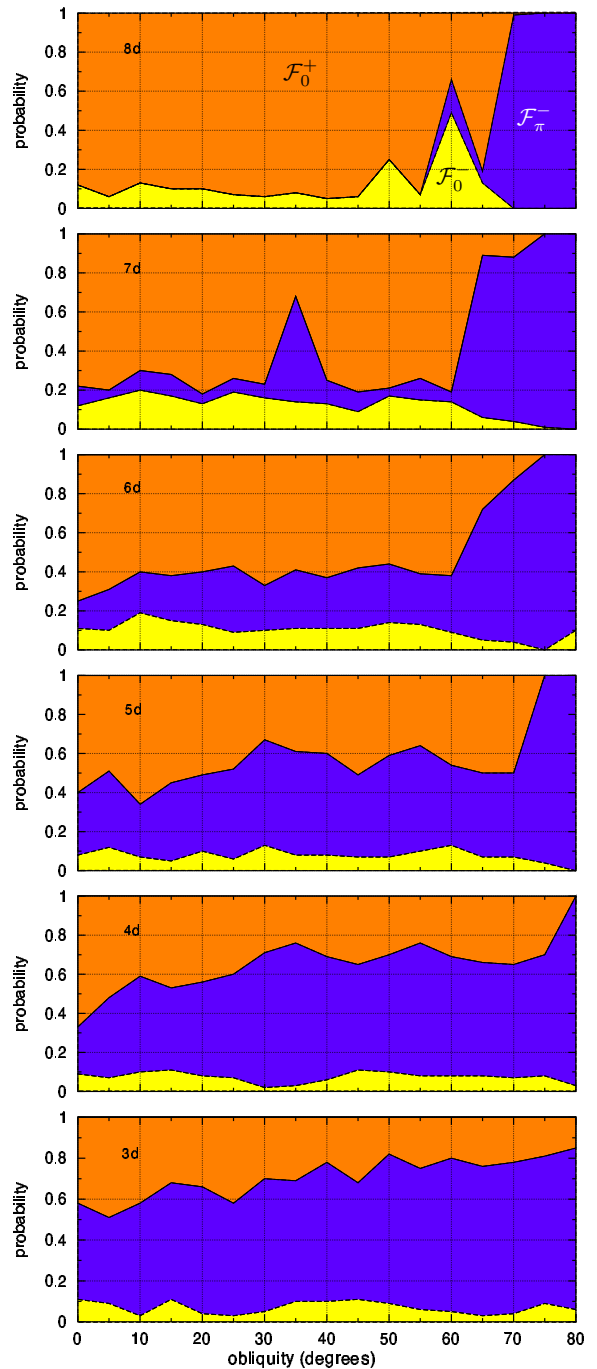

Figure 12: **Probability of ending in one of Venus' final states (grey: $\mathcal{F}_0^+$, light grey: $\mathcal{F}_0^-$, dark grey: $\mathcal{F}_\pi^-$).** For initial period of 3, 4, 5, 6, 7 and 8 days respectively, and initial obliquity from 0 to 80 degrees, with 5 degree step size, 100 trajectories have been computed with an increment of phase in the precession angle of 10^{-6} radian. These are the same kind of pictures as Fig. 4 in (V1). However, here there is a drastic reduction of $\mathcal{F}_0^-$ final states for slow initial rotation rates, because dissipation parameters of the standard model are weaker (see section 4).

13

If the motion is trapped in this island, we then say that there is a resonance between the secular frequency ν_k and the obliquity. The complete system is not integrable, as the terms in expression (11) are very numerous, but we can look individually to the location of each resonance. When the resonances are far apart, the motion will behave locally as in the integrable case, with just the addition of supplementary oscillations, but if several resonances overlap, the motion is no longer regular and becomes chaotic (Chirikov, 1979, see also Laskar, 1996).

2.6.2 The secular resonance s_8

Performing a frequency analysis (Laskar, 1990, 1999) of the obliquity over 20 Ma for Venus with $\alpha = 10"/\text{yr}$ we observe that for obliquities within $85° < \varepsilon < 90°$ there is an isolated resonance where the obliquity can be trapped, corresponding to the secular frequency s_8 (precession of the node of Neptune's orbit) (Fig. 13). With $s_8 \simeq -0.69"/\text{yr}$ (Table 3), for $\alpha_0 = 10"/\text{yr}$ (which corresponds to the initial period $\mathcal{P}_i \simeq 5$ d), we obtain from expression (12) an equilibrium obliquity $\varepsilon_e \simeq 86°$. As the rotation rate changes, so does α (see V2) and the equilibrium obliquity ε_e varies with ω as:

$$\cos \varepsilon_e = -\frac{2\omega\nu_k}{3n^2 E_d} . \qquad (14)$$

Therefore, we observe in Fig. 10 a slight curvature of the resonance strip, starting at about $85°$ for slow initial rotation periods and bending to $90°$, as the initial rotation period decreases.
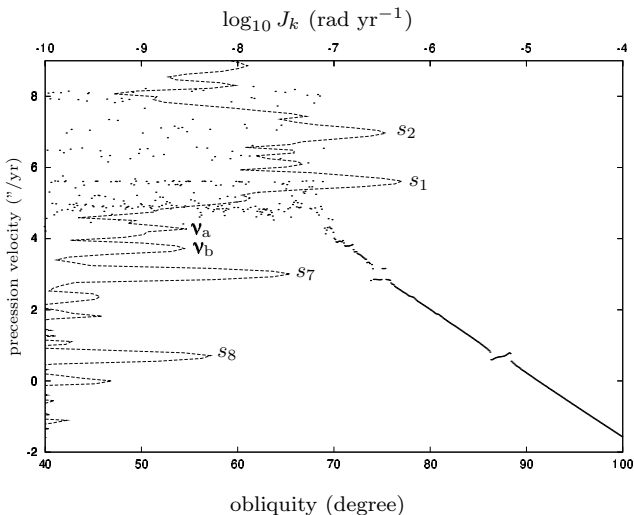

Figure 13: **Frequency analysis of the obliquity over 20 Ma for Venus with $\alpha = 10"/\text{yr}$.** The dotted line represents the spectrum of the secular perturbations (Table 3). For the frequency s_8, the frequency analysis proves the existence of a elliptic stability point for the obliquity close to $90°$ (Laskar and Robutel, 1993).

name	ν_k ("/yr)	J_k ("/yr)	ϕ_k (°)
s_2	-6.984	476.65×10^{-4}	-76.28
s_1	-5.589	829.74×10^{-4}	-106.33
ν_a	-4.280	5.29×10^{-4}	161.66
ν_b	-3.708	4.57×10^{-4}	40.53
s_7	-3.006	59.71×10^{-4}	50.07
s_8	-0.692	9.06×10^{-4}	-66.33

Table 3: **Principal secular frequencies of Venus' planetary perturbations orbit for slow precession speed ($\dot{\psi}$).**

2.6.3 Capture and escape probabilities

When dissipative torques are present, the existence of an isolated resonance is not sufficient to guarantee that the planet's obliquity will remain trapped. On the other hand, the same torques may allow non-resonant initial conditions to be captured into resonance after some time.

An overview of capture and escape probabilities was given in section 2.4 of (V2) for spin-orbit resonances. Here we are dealing with a different kind of resonances, but the same approach is still valid (for a review, see Henrard, 1993). A dissipation torque that provides a non zero capture probability (even for a small probability) is insufficient to lead a previously captured planet to escape from the resonance. Conversely, a torque that never allows the capture will always force the planet to leave the resonance. The only exception is a constant torque, but that is not the case of tidal and CMF torques. In Fig. 14, we plotted the probability of the planet's obliquity to be captured in a resonance as a function of the rotation period, in presence of gravitational and thermal atmospheric tides (CMF can be neglected for these rotation rates). Capture in the s_8 resonance subsists for a wide range of rotation periods. Thus, initial obliquities starting inside this resonance will remain captured until Venus enters in the slow rotation regime. Then, CMF effect becomes dominating (see Yoder, 1995a, 1997, V2) and the planet obliquity always abandon any previous resonant configuration. However, as the resonant obliquity remains inferior to $90°$, the planet will evolve into one of the final states with $\varepsilon = 0°$.

Although the s_8 resonance is quite resistant to tidal torques, there is only a small probability that Venus could be captured in this resonance ($P_{\text{cap.}} < 3\%$). This behavior can be observed in all numerical simulations including planetary perturbations (Figs. 15b, 15d, 16b, 16d, 19b, 19d, 17b, 22a, 22b and 22c). Indeed, for slow initial rotation periods and initial obliquities within about $60°$ and $90°$, we find sporadically some different final states than $\mathcal{F}_\pi^-$. Those exceptions correspond to trajectories that have experienced a capture in the s_8 resonance (Figs. 9e,g). Once captured, these trajectories remain inside the resonance until the slow rotation regime is reached. In order to get a numerical estimation of the
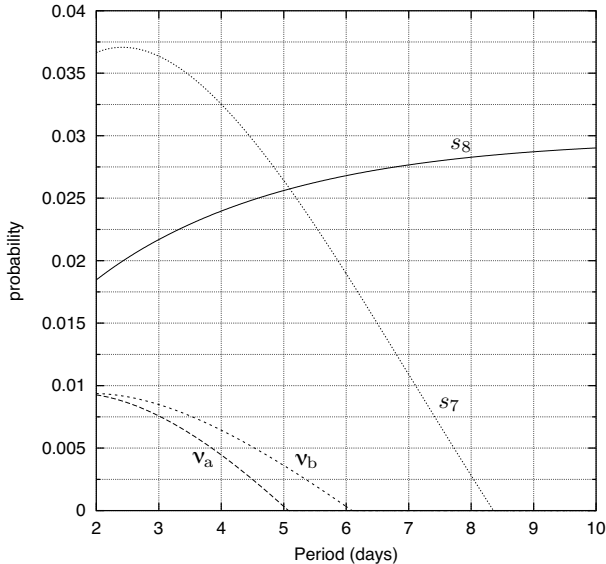
14

Figure 14: **Capture probabilities for secular resonances.** Each curve expresses the probability of the planet's obliquity of being captured in one resonance when crossing it, under the effect of gravitational and atmospheric tides. When the probability reaches zero, that also means that a previous captured obliquity will inevitably leave that resonance.

capture probabilities in the s_8 resonance, we run 1000 experiments starting close to the resonance. For each initial period and obliquity, we simultaneously integrated 100 orbits with initial precession angles separated by 0.05 rad (Table 4). About 3% of the trajectories were captured during the evolution, which is in a perfect agreement with the theoretical value of Fig. 14.

$\mathcal{P}_i$	ε_i	$\mathcal{F}_0^+$	$\mathcal{F}_0^-$	$\mathcal{F}_\pi^-$
7.0 d	70.0°	4	-	96
7.0 d	72.5°	4	-	96
7.0 d	75.0°	1	3	96
7.0 d	77.5°	1	1	98
7.0 d	80.0°	-	1	99
8.0 d	70.0°	5	2	93
8.0 d	72.5°	1	1	98
8.0 d	75.0°	3	1	96
8.0 d	77.5°	-	1	99
8.0 d	80.0°	2	-	98
Total (%)		2.1	1.0	96.9

Table 4: **Number of final evolutions which end in each final state for different initial conditions.** For the same initial period and obliquity we simultaneously integrated 100 orbits with initial precession angles separated by 0.05 rad. Final evolutions that end in a final state other than $\mathcal{F}_\pi^-$ correspond to a former capture in the s_8 resonance.

2.6.4 Other secular resonances

Besides s_8, the most significant secular frequencies are related to the precession of the node of the orbits of Mercury (s_1), Venus (s_2) and Uranus (s_7) (Fig. 13 and Table 3). s_1 and s_2 are in the large chaotic zone of the obliquity, preventing any kind of capture. However, for s_7 (and also for ν_a and ν_b) we may wonder if a similar behavior as for s_8 is possible, in spite of some small chaos already present in that area (visible in Fig. 13).

To answer to this question, we computed the dissipative torques in the vicinity of each resonance (Fig. 14). We see that contrarily to s_8, the capture probability for ν_a, ν_b and s_7 decreases rapidly to zero as the planet slows down. Thus, even if for some initial condition the motion is trapped in one of those resonances, and resisted to the chaotic diffusion, it will surely not resist to the dissipative torques. The secular resonance with s_8 is thus the only responsible for the exceptional behavior of initial conditions within $85° < \varepsilon < 90°$.

3 Parameter variations

Having described the behavior of the spin of Venus using the standard model, we will now perform some additional numerical experiments where one or several dissipation parameters of the standard model are modified. We will see that the main results depicted for the standard model will remain grossly unchanged, although some modifications will occur, especially in the case of a late formation of the atmosphere.

3.1 Tidal dissipation strength

For tidal dissipation we mean here the whole dissipation caused by gravitational and thermal atmospheric tides together. Indeed, as we have seen in (V2), within the constraint imposed by expression (7), those two effects can be described as a single one depending of the gravitational tidal model and dissipation factor Q.

In order to test expression (5), we chose a Q factor 50% larger than in the standard model (i.e. $Q_f = 60$ and $Q_n = 75$). The results are plotted in Fig. 15 for both the standard and the modified model. It is clear that the picture of the final spin evolution remain almost unchanged (except, of course, for solutions having crossed the chaotic zone). Moreover, the level lines indicating the time needed to reach a final state are grossly the same in both pictures, rescaled by a 1.5 factor in the modified model, corresponding to the 50% augmentation of the Q factor, in agreement with (5).

It should be noted that relation (5) was established in the particular case where the planet's obliquity was held fixed at $\varepsilon = 0°$ or $\varepsilon = 180°$, where the CMF cancels. However, since before approaching a final state, the planet
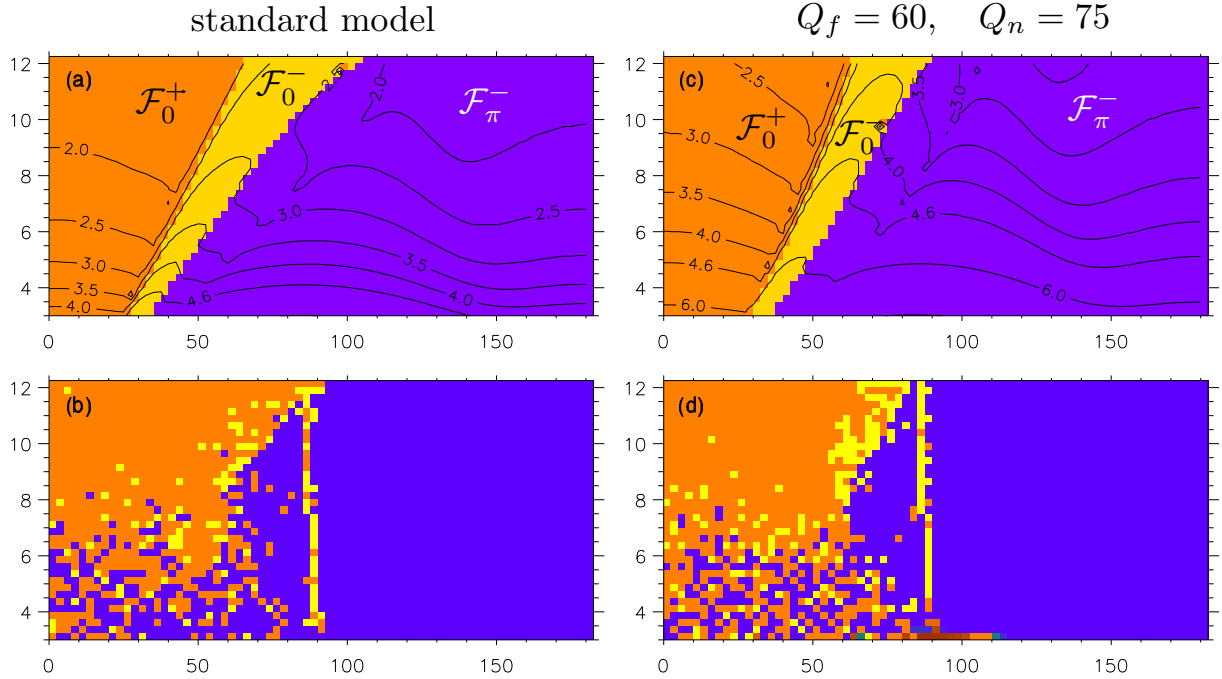
15

Figure 15: **Final states of Venus' spin for a planet less dissipative than in the standard model ($Q_f = 60$, $Q_n = 75$).** For initial obliquity ($\varepsilon_i \in [0°, 180°]$) and period ($\mathcal{P}_i \in [3\,\mathrm{d}, 12\,\mathrm{d}]$) we plotted the final evolutions for the standard model (left) and a planet less dissipative (right). The two pictures are almost identical (except for solutions having crossed the chaotic zone). The time needed to reach a final state is multiplied by a factor of 1.5 corresponding to the 50% augmentation of the Q factor.
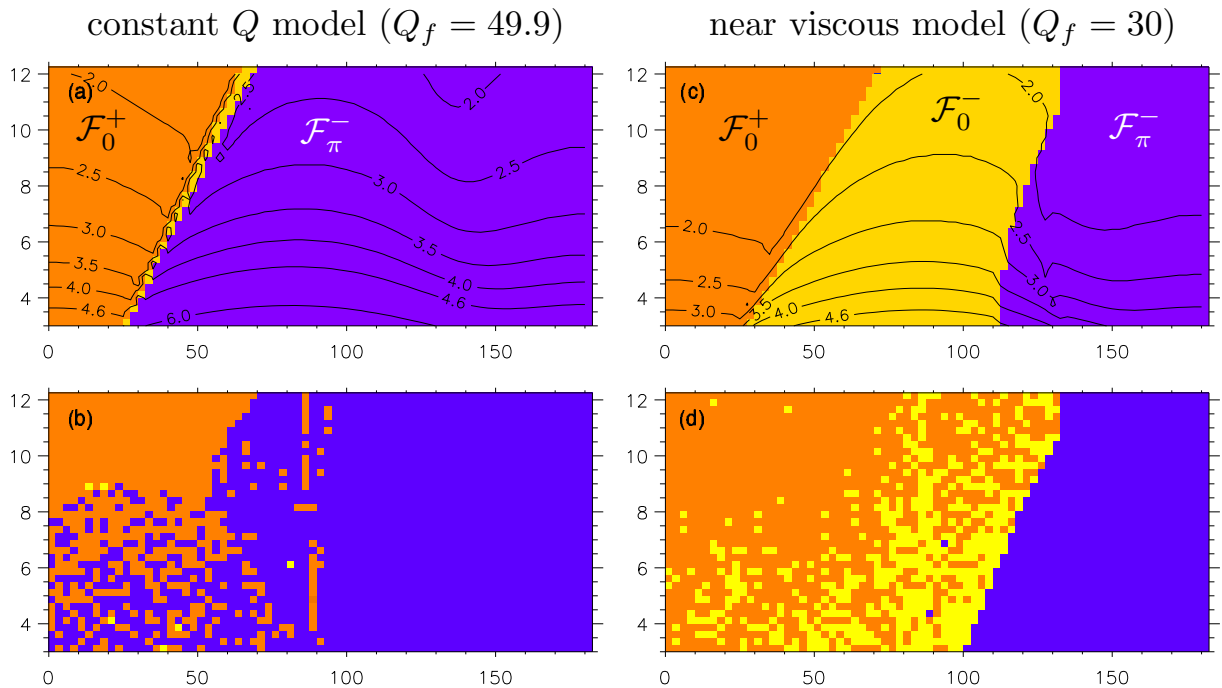

Figure 16: **Final states of Venus' spin for different tidal dissipation models.** For initial obliquity ($\varepsilon_i \in [0°, 180°]$) and period ($\mathcal{P}_i \in [3\,\mathrm{d}, 12\,\mathrm{d}]$) we plotted the final evolutions for the constant Q model (left) and for a more viscous model (right). The tidal model, mainly interferes with the number of retrograde final states of each kind: a constant Q model favors the final state $\mathcal{F}_\pi^-$, while the linear one favors the final state $\mathcal{F}_0^-$.

16

spends most of its evolution in a fast rotation regime, the CMF impact on the time evolution is negligible.

3.2 Change of tidal dissipation model

The tidal strength affects mainly the time needed to reach a final state. We will now see how the change of model affects the final picture. For the standard model, the dissipation is interpolated between the constant Q model and the viscous one, which can be retrieved by setting respectively $Q_f = Q_n$ or $Q_f \to 0$ in equation (2).

3.2.1 Constant Q model

The 'constant Q model' was used in most of the previous studies on Venus rotational evolution. Like Yoder (1995a, 1997) we set here $Q \simeq 50$ (more precisely, $Q_f = 49.9$ and $Q_n = 50$, to avoid singularities in our equations). With this model, we performed the same numerical experiment as in Fig. 15.

In absence of planetary perturbations (Fig. 16a), the most important difference from the standard model is the almost complete disappearance of the zone corresponding to the retrograde final states $\mathcal{F}_0^-$, which are now replaced by the $\mathcal{F}_\pi^-$. This happens because, when using the 'constant Q model', the amplitude of the atmospheric tides become almost infinite for tidal frequencies $\sigma = 0$, which prevents the rotation rate from evolving into negative values (Fig. 2). The time needed to reach the stabilization is also longer because $Q_f = 49.9$ corresponds to a weaker dissipation.

When planetary perturbations are added (Fig. 16b), we can isolate the same distinct three areas corresponding to different evolutions as in the standard model, though in the zone of mixed states, we practically find only the two final possibilities for the spin ($\mathcal{F}_0^+$ and $\mathcal{F}_\pi^-$).

3.2.2 Near viscous (or linear) model

The evolution of the tidal dissipation corresponding to a 'linear model' can be directly obtained from the expression of the interpolated model (Eq.2) setting $Q_f = 0$:

$$\lim_{Q_f \to 0} b^g(\sigma) = \frac{k_2 \sigma}{n Q_n} = k_2 \sigma \Delta t^g . \tag{15}$$

However, for fast rotation rates the gravitational tides dissipation becomes too strong, and incompatible with the condition (4). We thus preferred to use here an interpolated model, but which behaves like the linear model for a wider range of tidal frequencies than the standard one, choosing a fast dissipation factor $Q_f = 30$. The numerical results (Figs. 16c,d) give rise to a different kind of evolution. Indeed, in absence of planetary perturbations we observe a large augmentation of the retrograde states $\mathcal{F}_0^-$ zone, at the expense of the other retrograde final state $\mathcal{F}_\pi^-$.

The reason is the inverse as for the constant Q model: a linear model reduces the amplitude of the variations of the rotation rate ($\dot{\omega}$), and it becomes easier to cross the tidal frequencies $\sigma = 0$. Also, as the dissipation is stronger, gravitational tides acting before the formation of the atmosphere are able to lower rapidly the obliquities.

The minimal critical initial obliquity which allows an evolution into the retrograde final state $\mathcal{F}_\pi^-$ is now always higher than $100°$, that is, about $10°$ more than the boundaries of the chaotic zone. Once the effects of planetary perturbations are taken into account, in the zones of mixed states, we only count the two final states $\mathcal{F}_0^+$ and $\mathcal{F}_0^-$, since the retrograde final states $\mathcal{F}_\pi^-$ cannot be reached by simple diffusion in the chaotic zone. In addition, we also observe that the entire zone corresponding to the retrograde final states $\mathcal{F}_0^-$ in the non perturbed case, is replaced by a mixed zone, even for slow initial rotation periods and high initial obliquities. Indeed, most of the paths leading to the final state $\mathcal{F}_0^-$ are close to the paths leading to $\mathcal{F}_0^+$ (Fig. 3), and even a short journey of the obliquity in the chaotic zone is enough to exchange these two evolutions. We thus find that a constant Q model favors the final state $\mathcal{F}_\pi^-$, while the linear one favors $\mathcal{F}_0^-$.

3.3 Atmosphere

In the standard model, we considered that the effect of the atmosphere starts 300 million years after the planetary formation and grows linearly to the present values within 500 million years (Eq.8). To analyze the consequences of its formation date on the dynamical evolution of the spin, we have plotted in figure 17 the evolution for a late formation of a dense atmosphere. In this example, we assume that the formation of the atmosphere only starts after the end of the last heavy bombardment (some 800 million years after the Solar System formation) and that the present stage is attained in 200 million years, that is with a weight function $\zeta(t)$ (see Eq.8),

$$\zeta(t) = \begin{cases} 0 & \text{if} & t \leq 0.8\,\text{Ga} \\ (t_{\text{Ga}} - 0.8)/0.2 & \text{if} & 0.8\,\text{Ga} < t < 1.0\,\text{Ga} \\ 1 & \text{if} & t \geq 1.0\,\text{Ga} \end{cases} \tag{16}$$

In absence of planetary perturbations (Fig. 17a), and for initial rotation periods faster than about $\mathcal{P}_i = 7$ days, the results are similar to those of the standard model (Fig. 4). Indeed, for a fast rotating planet ($\omega \gg n$), the effect of the atmosphere on the rotation rate can be neglected. There still remains, even for fast rotation rates, a small contribution to the obliquity (see V2), and we can observe a slight displacement to the right of the critical obliquities separating the different final states zones. This difference becomes larger as the initial rotation gets slower. For $\mathcal{P}_i \simeq 9$ days and $\varepsilon \simeq 135°$, we have a sudden modification in the shape of the separating line between the two retrograde
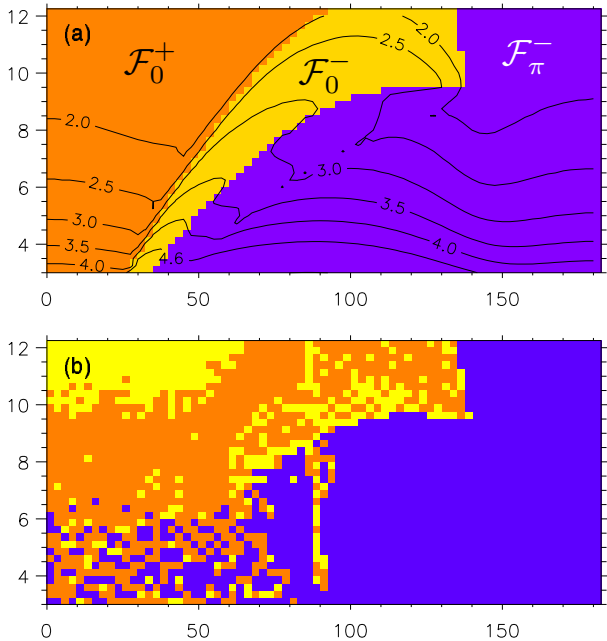
late atmosphere (0.8 → 1.0 Ga)

Figure 17: **Final states of Venus' spin for a late formation of the atmosphere.** For initial obliquity ($\varepsilon_i \in [0°, 180°]$) and period ($\mathcal{P}_i \in [3\,\mathrm{d}, 12\,\mathrm{d}]$) we plotted the final evolutions for an atmosphere that starts its accretion 800 million years after the Solar System formation and that attains its present stage in 200 million years. In the upper left corner of the perturbed picture (b), we notice the presence of a large number of the retrograde final states $\mathcal{F}_0^-$ due to a previous passage trough the 1:1 resonance.

final states $\mathcal{F}_0^-$ and $\mathcal{F}_\pi^-$. This apparent discontinuity is linked to the date of the atmosphere's formation. Before 0.8 Ga, for those initial conditions, the obliquity has already attained a temporary equilibrium position ε_e due to gravitational tides alone (V2, Eq.69):

$$\varepsilon_e = \arccos\left(2n/\omega\right) . \tag{17}$$

As soon as the effect of the atmosphere begins, this equilibrium is disrupted and the obliquity starts to change again.

When planetary perturbations are added (Fig. 17b), for initial rotation periods faster than $\mathcal{P}_i = 7$ days we observe similar patterns as for the standard model (Fig. 10). As in Fig. 16d, the zones previously occupied by the retrograde final state $\mathcal{F}_0^-$ are transformed in zones of mixed states $\mathcal{F}_0^+$ and $\mathcal{F}_0^-$. Nevertheless, in the upper left corner of Fig. 17b, normally fully occupied by the direct rotation final states $\mathcal{F}_0^+$, we notice the presence of a large number of retrograde final states $\mathcal{F}_0^-$. This remarkable phenomenon was first seen in (V1) and it was explained in detail in (V2). For a late introduction of the atmosphere, tidal dissipation can slow down the planet to the synchronous rotation state. However, due to the permanent CMF effect resulting from

the forced obliquity induced by planetary perturbations, Venus has a great probability of skipping this resonance and continue to slow down to an equilibrium rotation rate $\omega_e < n$ such that (V2, Eq.116):

$$\omega_e \simeq n(1 - \varrho\delta\varepsilon^2) . \tag{18}$$

Once the atmospheric torque becomes important, the planet will evolve into the final state $\mathcal{F}_0^-$ according to the evolutionary tendencies plotted in Fig. 2a. For the standard model, the probability of capture in the 1:1 resonance is very small, as it is show in Fig. 18. Nevertheless, even when the capture in the resonance occurs, the atmospheric torque obliges the planet to leave the previous equilibrium state (see V2, section 4.6.2). The later is the formation of the atmosphere (or stronger is the dissipation), the larger is the zone occupied by the $\mathcal{F}_0^-$ final states in the top of the picture, as we will see in section 4 (Figs. 22, 23).
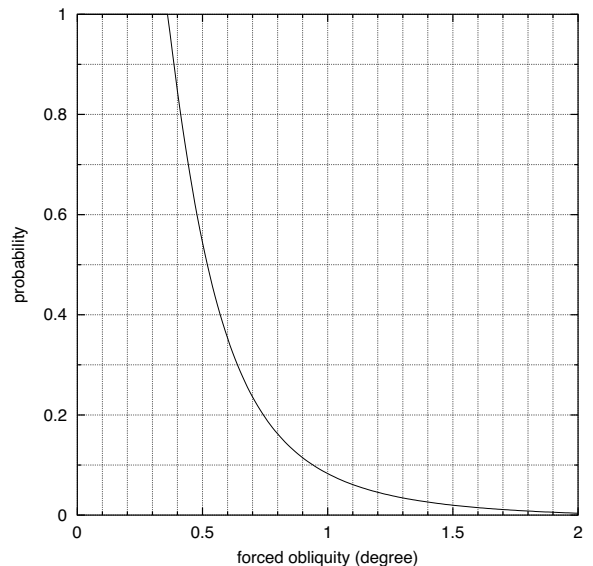

Figure 18: **Probability of capture in the 1:1 resonance.** Using the dissipation parameters of the standard model, we plotted the capture probability of the planet as a function of the forced obliquity $\delta\varepsilon$. (V2, Eq.120).

3.4   Core-mantle friction

The difficulty in modeling the CMF effect comes essentially from two unknown parameters: the effective viscosity ν and the non-hydrostatic core ellipticity δE_c. The uncertainty on δE_c is about one order of magnitude, while ν covers thirteen orders of magnitude (Lumb and Aldridge, 1991). However, E_c appears as a square (cube in the turbulent regime) in the dynamical equations, while the effective viscosity enters as a square root (V2, Eq.52). This

18

reduces the impact of ν, but increases it for E_c. Their contribution to the Reynolds' number (Re) is (V2, Eqs.55, 56):

$$\mathrm{Re} = \frac{(\alpha R_c \cos \varepsilon \sin \varepsilon)^2}{\omega \nu E_c^2} \;, \tag{19}$$

where R_c is the planet's core radius. Turbulence usually sets in for $\mathrm{Re} \sim 10^5$ to 10^6. Thus, high values of ν and E_c delay turbulent friction, but since the doubtfulness upon ν is about six times greater than for E_c^2, it is essentially the effective viscosity that determines the onset of turbulence.

3.4.1 Effective viscosity

In order to estimate the consequences of the effective viscosity in the final evolution of Venus, we performed two experiments, with $\nu = 10^{-4}\,\mathrm{m^2\,s^{-1}}$ and $\nu = 10^{-2}\,\mathrm{m^2\,s^{-1}}$ (Fig. 19). We observe two distinct behaviors. For $\nu = 10^{-4}\,\mathrm{m^2\,s^{-1}}$ (left hand side pictures) we hardly differentiate the results from those of the standard model (where $\nu = 10^{-6}\,\mathrm{m^2\,s^{-1}}$), which contrasts with the case where $\nu = 10^{-2}\,\mathrm{m^2\,s^{-1}}$ (right hand side pictures).

For small values of the effective viscosity, the CMF effect only becomes important for slow rotation rates, after the onset of turbulence (only the time needed to reach the final states is little shorter). We plotted in Fig. 21, the change of the different coupling parameters κ with the rotation rate ω. According to the definition of the transition Reynolds number (R_T) given in (V2, Eq.76), the onset of turbulence always occurs at the intersection of $\kappa(\mathrm{lam.})$ with $\kappa(\mathrm{turb.})$. Thus, for a giving ν value, the correct coupling parameter κ to use in the dynamical equations is given by the maximal value of $\kappa(\mathrm{lam.})$ and $\kappa(\mathrm{turb.})$. Usually, for $\delta E_c \simeq 4\delta E_d$, the CMF effect becomes efficient for ω values within $3n$ and $4n$, that is, for $\log_{10}(\omega/n) \sim 0.5$. Since, for $\nu = 10^{-4}\,\mathrm{m^2\,s^{-1}}$ and $\nu = 10^{-6}\,\mathrm{m^2\,s^{-1}}$ the onset of turbulence occurs in the fast rotation regime, the main contribution of these two CMF effects to dynamical equations is thus identical and the final picture remains essentially unchanged.

On the other hand, for $\nu = 10^{-2}\,\mathrm{m^2\,s^{-1}}$, the onset of turbulence occurs in the slow rotation regime. This means that when CMF effect becomes efficient, the friction is still laminar, and therefore stronger than it was in the previous situations. The main consequence will be a strong reduction in the number of the retrograde final states $\mathcal{F}_0^-$. Indeed, since the CMF effect is much more efficient here than in the standard model, it will quickly bring the obliquity into one of its stability points ($\varepsilon = 0°$ or $\varepsilon = 180°$), preventing the rotation rate ω to become smaller than n. As a consequence, when planetary perturbations are considered, the zone of mixed states is predominantly occupied by the two final states $\mathcal{F}_0^+$ and $\mathcal{F}_\pi^-$.
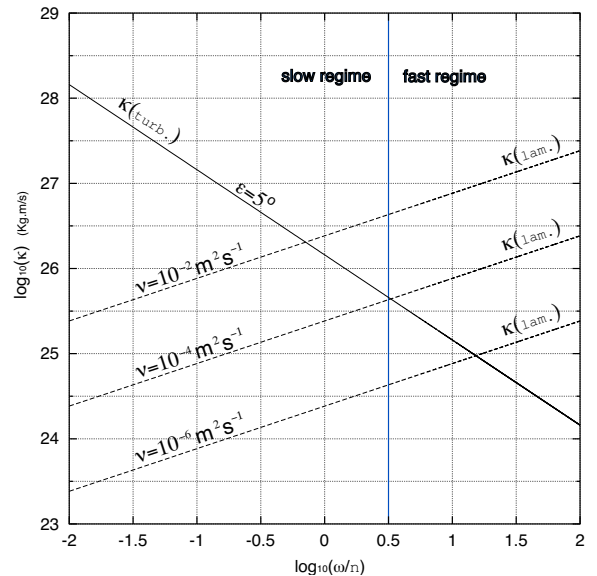

Figure 21: **Variation of the coupling parameter κ with the rotation rate.** Each line represents κ for different values of the effective viscosity and in two different regimes. The onset of turbulence always occurs in the interception of $\kappa(\mathrm{lam.})$ with $\kappa(\mathrm{turb.})$. Then, for a giving ν value, the correct coupling parameter κ to take into dynamical equations is given by the maximal value of $\kappa(\mathrm{lam.})$ and $\kappa(\mathrm{turb.})$. We used $\delta E_c \simeq 4\delta E_d$ (Herring *et al.*, 1986).

3.4.2 Core ellipticity

The effect of the core ellipticity E_c is opposite to the effect of the effective viscosity ν. Moreover, according to expression (19), a smaller value of E_c anticipates the onset of turbulence, giving rise to a dependency of dynamical equations in E_c^{-3}. In Figs. 20a,b we plotted the results of a numerical simulation where the non-hydrostatic core ellipticity is $\delta E_c = 2.5 \times 10^{-5}$, that is, twice smaller than for the standard model. The CMF effect is thus stronger, and we obtain an identical behavior as for a strong effective viscosity (Figs. 19c,d). However, in presence of planetary perturbations (Fig. 20b), the final states are more scattered than in the case of a strong effective viscosity (Fig. 19d). In fact, for a small core ellipticity, when planetary perturbation are not present, the critical obliquities for transition into the different final states, correspond to lower initial obliquities.

Another important difference between the two cases is the presence, in the upper left corner of Fig. 20b, of a concentration of retrograde final state $\mathcal{F}_0^-$, in a similar way as for a late introduction of the atmosphere (Fig. 17b). Here, the atmosphere grows at the same rate as in the standard model, but the stronger CMF decelerates much faster the low initial obliquities (that wander in the chaotic zone), allowing initial conditions with slowest period to approach the synchronous rotation state before 300 Ma.
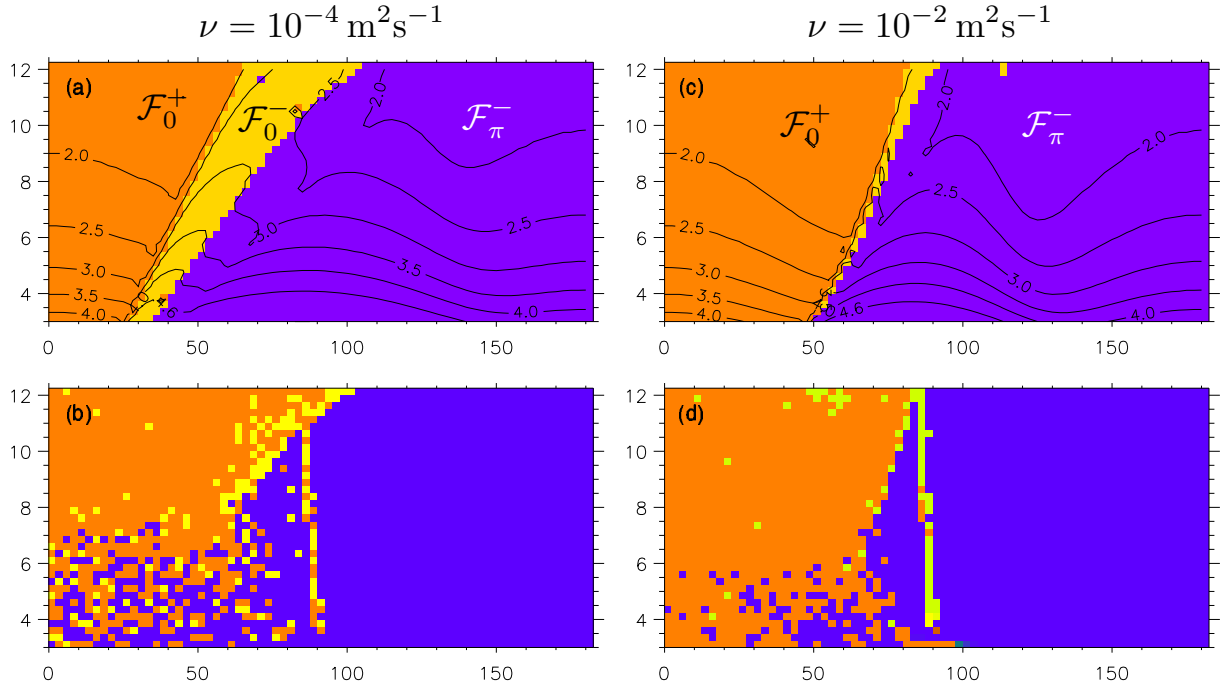
19

Figure 19: **Final states of Venus' spin for different CMF effective viscosities.** For initial obliquity ($\varepsilon_i \in [0°, 180°]$) and period ($\mathcal{P}_i \in [3\,\mathrm{d}, 12\,\mathrm{d}]$) we plotted the final evolutions for $\nu = 10^{-4}\,\mathrm{m^2\,s^{-1}}$ (left) and for $\nu = 10^{-2}\,\mathrm{m^2\,s^{-1}}$ (right). In the first case the final picture resemble the standard model (Fig. 15a,b) because CMF friction is essentially turbulent, therefore, independent of ν. However, for $\nu = 10^{-2}\,\mathrm{m^2\,s^{-1}}$, CMF is still laminar in the slow rotation regime, then stronger than in the standard model (Fig. 21).
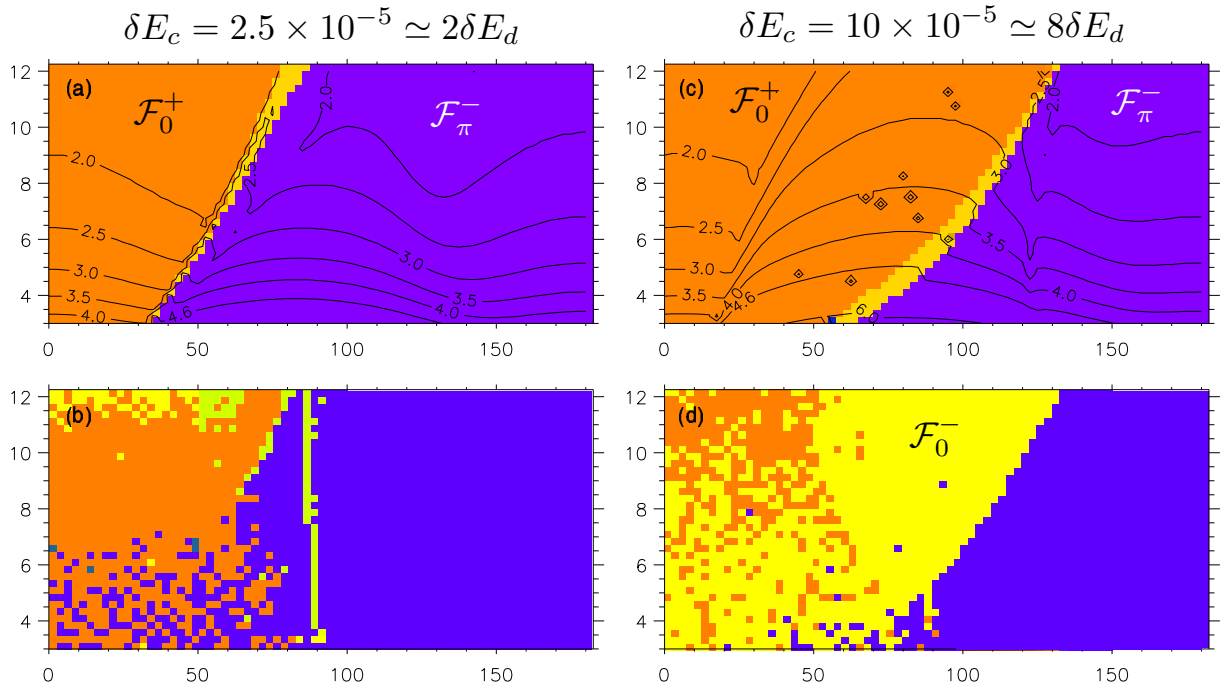

Figure 20: **Final states of Venus' spin for different CMF core non-hydrostatic ellipticity.** For initial obliquity ($\varepsilon_i \in [0°, 180°]$) and period ($\mathcal{P}_i \in [3\,\mathrm{d}, 12\,\mathrm{d}]$) we plotted the final evolutions for $\delta E_c = 2.5 \times 10^{-5} \simeq 2\delta E_d$ (left) and for $\delta E_c = 10 \times 10^{-5} \simeq 8\delta E_d$ (right). The effect of E_c is opposite to the effect of ν: a small E_c increases the strength of the CMF effect. In presence of planetary perturbations (b,d) we notice the presence of a large number of retrograde final states $\mathcal{F}_0^-$, though due to different reasons in each case: a previous passage through the 1:1 resonance (left) and a small critical obliquity (right).

In Figs. 20c,d, we have chosen a non-hydrostatic core ellipticity $\delta E_c = 10^{-4}$, twice larger than for the standard model. This reduces substantially the CMF effect, which is only present for very slow rotation rates. The late appearance of a strong CMF causes the planet to take more time to reach a final state (given by the labeled lines). Usually, the final states $\mathcal{F}_0^-$ are associated with this augmentation in the stabilization time, but in absence of planetary perturbations (Fig. 20c), the retrograde final states $\mathcal{F}_0^-$ almost disappear. This is because close to the critical points $\sigma = 0$ (in particular for $\omega = n$), the CMF in the turbulent regime is not strong enough to counterbalance the effect of atmospheric tides (see Fig. 2). However, once planetary perturbations are considered (Fig. 20d), the CMF effect is increased during the passage through the critical points $\sigma = 0$ (see V2, section 4.5) and the retrograde final states $\mathcal{F}_0^-$ regain a large portion of the final evolutions.

4 Stronger dissipation

The results presented in the previous sections for the long-term evolution of Venus, are in good agreement with the results from (V1). In the final evolution picture, we always count three distinct zones: for high initial obliquities, a large area corresponding to the retrograde final state $\mathcal{F}_\pi^-$; for low initial obliquities and fast initial rotation rates, a zone of mixing final states; and the remaining area, where the direct rotation final states $\mathcal{F}_0^+$ are prevailing. The main difference with respect to (V1) concerns this last area, where we found in (V1) a large zone of retrograde final states $\mathcal{F}_0^-$ (Fig. 22c). As explained in section 3.3, this behavior corresponds to a previous passage through the synchronous resonance. This was made possible because in (V1) the effect of the atmosphere is only considered after 1.0 Ga, and because all the dissipative parameters are stronger than in the present standard model ($Q_f = 21.5$, $\nu = 10^{-2}\,\mathrm{m^2\,s^{-1}}$, $\delta E_c = 9.75 \times 10^{-6}$).

In Fig. 22a we plotted the final evolutions picture in presence of planetary perturbations for a dissipation model like the standard one, but where $Q_f = 21.5$ and $\nu = 10^{-2}\,\mathrm{m^2\,s^{-1}}$. Results are now shown starting at the initial period $\mathcal{P}_i = 2$ days, since the stronger dissipation allows faster initial periods. The final picture is more or less a combination of the scenarios of Fig. 16d ($Q_f = 30$) and Fig. 19d ($\nu = 10^{-2}\,\mathrm{m^2\,s^{-1}}$), but in the top left corner of this figure we notice the presence of the retrograde final state $\mathcal{F}_0^-$, as it was observed in Fig. 17b (late introduction of the atmosphere) and in Fig. 20b (small core ellipticity). The atmosphere model is still the one of the standard model (8), but the stronger dissipation allows the paths with slow initial periods to skip the 1:1 resonance, before the effect of the atmosphere becomes efficient. In Fig. 22b, we use the same choice of parameters as for Fig. 22a, ex-
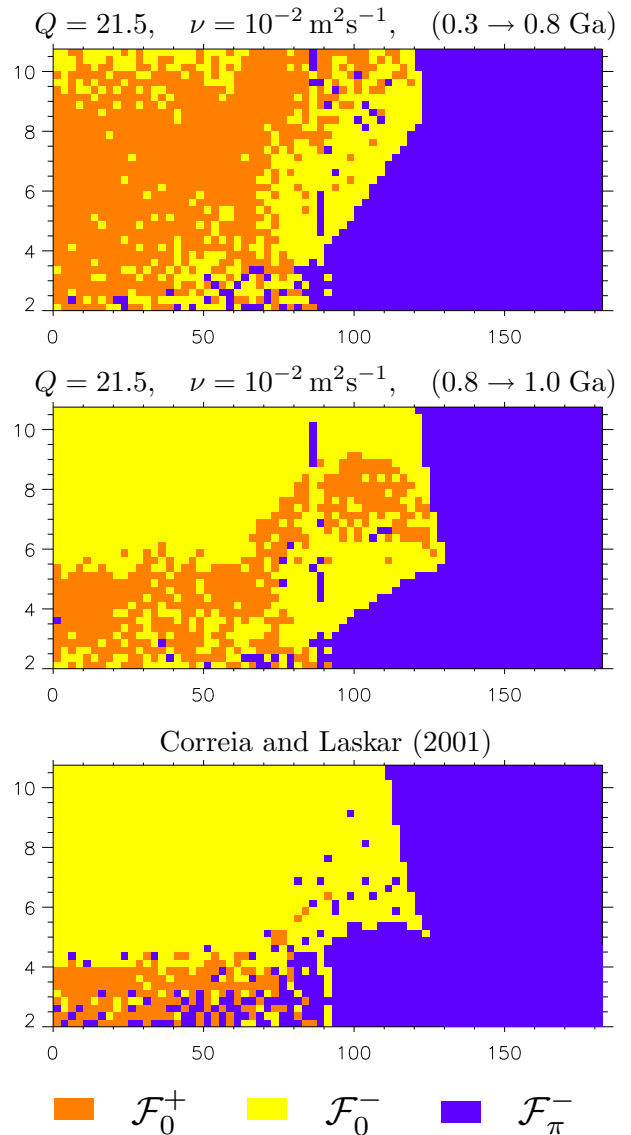

$Q = 21.5, \quad \nu = 10^{-2}\,\mathrm{m^2 s^{-1}}, \quad (0.3 \to 0.8\,\mathrm{Ga})$

$Q = 21.5, \quad \nu = 10^{-2}\,\mathrm{m^2 s^{-1}}, \quad (0.8 \to 1.0\,\mathrm{Ga})$

Correia and Laskar (2001)

$\mathcal{F}_0^+ \qquad \mathcal{F}_0^- \qquad \mathcal{F}_\pi^-$

Figure 22: **Final states of Venus' spin for strong dissipation models.** For initial obliquity ($\varepsilon_i \in [0°, 180°]$) and period ($\mathcal{P}_i \in [2\,\mathrm{d}, 10.5\,\mathrm{d}]$) we plotted the final evolutions for a successive increase in the dissipation models and the date of the formation of the atmosphere. We notice a progressive replacement of the number of direct rotation final states $\mathcal{F}_0^+$ by the retrograde final states $\mathcal{F}_0^-$.

cept for the formation of the atmosphere, which is given by expression (16). Thus, with the combination of a strong dissipation with a late atmosphere, we observe like in (V1) an almost total replacement of the direct final state $\mathcal{F}_0^+$ zone, by a zone of retrograde final states $\mathcal{F}_0^-$ (to be compared with Fig. 22c).
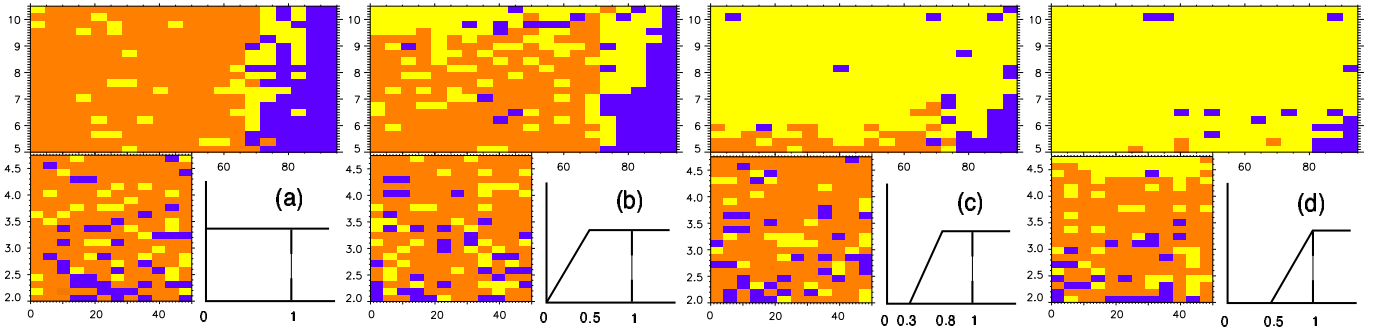
Figure 23: **Final states of Venus' spin for different atmosphere evolutions.** For initial obliquity ($\varepsilon_i \in [0°, 180°]$) and period ($\mathcal{P}_i \in [2\,\mathrm{d}, 10.5\,\mathrm{d}]$) we plotted the final evolutions for a successive increase the date of the formation of the atmosphere using the same dissipation parameters from Correia and Laskar (2001). In (a) the atmosphere is present from the beginning of the evolution. In (b), (c) and (d) the atmosphere density grows linearly during 0.5 Ga, but starting at different epochs. We notice a progressive replacement of the number of direct rotation final states $\mathcal{F}_0^+$ by the retrograde final states $\mathcal{F}_0^-$.

4.1 Introduction of the atmosphere

To stress the importance of the date of formation of the atmosphere on Venus, in the case of a planet with a strong dissipation, we performed a last set of numerical simulations, using the same dissipative model and parameters as in (V1), but introducing the atmosphere at different epochs (Fig. 23). In (V1) (Fig. 22c), the atmosphere was abruptly introduced 1 Ga after the formation of the planet. In fact, the final picture does not change much for a linear introduction of the atmosphere between 0.5 and 1.0 Ga (Fig. 23d). When the atmosphere is present from the very beginning (Fig. 23a), we observe that the large area occupied by the retrograde rotation final states $\mathcal{F}_0^-$ is replaced by a region where the direct rotation final state $\mathcal{F}_0^+$ dominates (although $\mathcal{F}_0^-$ is still present), in a similar way as for the standard model. Indeed, since the atmosphere is present from the beginning, the planet never approaches the synchronous rotation state, in spite of the strong dissipation. However, when the atmosphere formation is delayed (Figs. 23b-d), the zone of retrograde final states $\mathcal{F}_0^-$ increases, in an identical replacement sequence as in Figs. 22a-c.

5 Conclusions

One of the main difficulties for the understanding of the long term evolution of the spin of Venus arises from the uncertainty of many of the involved geophysical parameters. In the present study, we have chosen a set of parameters which we believe to represent the most plausible values for our current understanding of the planet. We called this model the 'standard model'. Its evolution is analyzed here in full details, but as some of its parameters are only loosely constrained, we also discussed the impact of their possible variations. One of our main results is that in all

cases but one, the spin of Venus can always reach three of the four final states of Venus (one of direct rotation, $\mathcal{F}_0^+$, and two of retrograde rotation, $\mathcal{F}_0^-$ and $\mathcal{F}_\pi^-$). The only exception is the scenario with a constant Q model (see section 3.2.1), where the final state $\mathcal{F}_0^-$ is not attainable. Although it was used in most of the previous studies on Venus, we believe that this model is not realistic for slow rotation rates, as the amplitude of thermal atmospheric tides becomes infinite for a zero tidal frequency ($\sigma = 0$), which prevents the CMF to reduce the rotation rate to $\omega < n$. Thus, we do not recommended to use this model in further studies of slow rotating planets like Venus.

The consideration of the resonances between the precession frequency and the secular orbital frequencies, has proven to be essential in the search for realistic scenarios of evolution. Apart from the important effect of the crossing of the chaotic zone (Laskar and Robutel, 1993), a striking example is given by the secular resonance between the obliquity and the precession of the node of Neptune's orbit, which modifies the distribution of final states for trajectories captured in this resonance. Furthermore, the planetary perturbations eliminate the constraint upon the critical obliquity that allows the evolution into a retrograde final state. Indeed, as long as a trajectory crosses the chaotic zone during its evolution, any of the three possible final spin evolutions can be expected, provided that the critical obliquities lie inside this chaotic zone. This is frequently the case, especially for a planet with fast initial rotation.

In the present study, we have restricted our analysis to initial rotation periods slower than 2 or 3 days. One may question this choice as many of the Solar System planets present a faster spin in our days. In fact, the initial rotation period of Venus can be chosen as fast as we desire, as long as we increase the dissipation, in order to reach the present configuration within the age of the Solar System. This could be possible during the first billion years as

proposed by several authors (eg. Burns, 1976, Lambeck, 1980), while some additional possibilities comes from the recent work of Touma and Wisdom (2001). A scenario with a faster initial period and a stronger dissipation can be easily deduced with some proper rescaling of the various scenarios presented here (Eq.5), and it should not modify substantially the general picture which is given in the present work, which already revealed to be robust to changes of parameters or models.

Acknowledgments

References

Avduevskii, V.S., Golovin, Iu.M., Zavelevich, F.S., Likhushin, V.Ia., Marov, M.Ia., Melnikov, D.A., Merson, Ia.I., Moshkin, B.E., Razin, K.A., and Chernoshchekov, L.I. 1976. Preliminary results of an investigation of the light regime in the atmosphere and on the surface of Venus. *Kosmicheskie Issledovaniia* **14**, 735-742.

Burns, J.A. 1976. Consequences of the tidal slowing of Mercury. *Icarus* **28**, 453-458.

Busse, F.H. 1968. Steady fluid flow in a precessing spheroidal shell. *J. Fluid Mech.* **33**, 739-751.

Chirikov, B.V. 1979. A universal instability of many dimensional oscillator systems. *Physics Reports* **52**, 263-379.

Chyba, C.F. 1987. The cometary contribution to the oceans of primitive Earth. *Nature* **330**, 632-635.

Colombo, G. 1966. Cassini's second and Third Laws. *Astron. J.* **71**, 891-896.

Correia, A.C.M., and Laskar, J. 2001. The four final rotation states of Venus. *Nature* **411**, 767-770.

Correia, A.C.M., Laskar, J., and Néron de Surgy, O. 2002. Long term evolution of the spin of Venus - Theory. *submitted to Icarus* , .

Dickey, J.O., Bender, P.L., Faller, J.E., Newhall, X.X., Ricklefs, R.L., Ries, J.G., Shelus, P.J., Veillet, C., Whipple, A.L., Wiant, J.R., Williams, J.G., and Yoder, C.F. 1994. Lunar Laser Ranging - a Continuing Legacy of the Apollo Program. *Science* **265**, 482-490.

Dobrovolskis, A.R., and Ingersoll, A.P. 1980. Atmospheric tides and the rotation of Venus. I - Tidal theory and the balance of torques. *Icarus* **41**, 1-17.

Dobrovolskis, A.R. 1980. Atmospheric tides and the rotation of Venus. II - Spin evolution. *Icarus* **41**, 18-35.

Dones, L., and Tremaine, S. 1993. On the origin of planetary spins. *Icarus* **103**, 67-92.

Gans, R.F. 1972. Viscosity of the Earth's core. *J. Geophys. Res.* **77**, 360-366.

Gold, T., and Soter, S. 1969. Atmospheric tides and the resonant rotation of Venus. *Icarus* **11**, 356-366.

Goldreich, P., and Soter, S. 1966. Q in the Solar System. *Icarus* **5**, 375-389.

Goldreich, P., and Peale, S.J. 1970. The obliquity of Venus. *Astron. J.* **75**, 273-284.

Hart, M.H. 1978. The evolution of the atmosphere of the Earth. *Icarus* **33**, 23-39.

Henrard, J. 1987. Colombo's Top. *Celest. Mech. & Dyn. Astron.* **40**, 345-366.

Henrard, J. 1993. The adiabatic invariant in classical dynamics. *Dynamics Reported*, pp. 117-235. Springer Verlag, New York.

Herring, T.A., Gwinn, C.R., and Shappiro, I.I. 1986. Geodesy by radio interferometry: Studies of the forced nutations of the earth. I - Data analysis. II - Interpretation. *J. Geophys. Res.* **91**, 4755-4765.

Hide, R. 1969. Interaction between the Earth's liquid core and solid mantle. *Nature* **222**, 1055-1056.

Hunten, D.M. 1993. Atmospheric evolution of the terrestrial planets. *Science* **259**, 915-920.

Kasting, J.F. 1993. Earth's early atmosphere. *Science* **259**, 920-925.

Konopliv, A.S., and Yoder, C.F. 1996. Venusian k2 tidal Love number from Magellan and PVO tracking data. *Geophys. Res. Lett.* **23**, 1857-1860.

Kundt, W. 1977. Spin and atmospheric tides of Venus. *Astron. Astrophys.* **60**, 85-91.

Lago, B., and Cazenave, A. 1979. Possible dynamical evolution of the rotation of Venus since formation. *The Moon and the planets* **21**, 127-154.

Lambeck, K. 1980. *The Earth's Variable Rotation*. Cambridge University Press, Cambridge.

Lambeck, K. 1988. *Geophysical Geodesy*. Oxford University Press, Oxford.

Laskar, J. 1990. The chaotic motion of the solar system. *Icarus* **88**, 266-291.

Laskar, J., Robutel, P. 1993. The chaotic obliquity of the planets. *Nature* **361**, 608-612.

Laskar, J. 1994. Large-scale chaos in the Solar System. *Astron. Astrophys.* **287**, L9-L12.

Laskar, J. 1996. Large scale Chaos and marginal stability in the Solar System. *Celest. Mech. & Dyn. Astron.* **64**, 115-162.

Laskar, J. : 1999, Introduction to frequency map analysis, *in proc. of NATO ASI Hamiltonian Systems with Three or More Degrees of Freedom, C. Simò ed, Kluwer*, (134-150)

Lumb, L.I., and Aldridge, K.D. 1991. On viscosity estimates for the Earth's fluid outer core-mantle coupling. *J. Geophys. Geoelectr.* **43**, 93-110.

McNamee, J.B., Borderies, N.J., and Sjogren, W.L. 1993. Venus - Global gravity and topography. *J. Geophys. Res.* **98**, 9 113-9 128.

McCue, J., and Dormand, J.R. 1993. Evolution of the spin of Venus. *Earth, Moon, & Plan.* **63**, 209-225.

McDonald, G.J.F. 1964. The friction. *J. Geophys. Res.* **2**, 467-541.

Melosh, H.J., Vickery, A.M. 1989. Impact erosion of the primordial atmosphere of Mars. *Nature* **338**, 487-489.

Melton, C.E., and Giardini, A.A. 1982. The evolution of the Earth's atmosphere and oceans. *Geophys. Res.h Lett.* **9**, 579-582.

Néron de Surgy, O. 1996. *Influence des effets dissipatifs sur les variations à long terme des obliquités planétaires.* Observatoire de Paris.

Néron de Surgy, O., and Laskar, J. 1997. On the long term evolution of the spin of the Earth. *Astron. Astrophys.* **318**, 975-989.

Pepin, R.O. 1991. On the origin and early evolution of terrestrial planet atmospheres and meteoritic volatiles. *Icarus* **92**, 2-79.

Pepin, R.O. 1994. Evolution of the martian atmosphere. *Icarus* **111**, 289-304.

Poirier, J.P. 1988. Transport properties of liquid metals and the viscosity of the Earth's core. *Geophys. J.* **92**, 99-105.

Roberts, P.H., and Stewartson, K. 1965. On the motion of a liquid in a spheroidal cavity of a precessing rigid body, II. *Proc. Camb. Phil. Soc.* **61**, 279-288.

Rochester, M.G. 1976. The secular decrease of obliquity due to dissipative core-mantle coupling. *Geophys. J.R.A.S.* **46**, 109-126.

Sasao, T., Okubo, S., and Saito, M. 1980. Linear theory on the dynamical effects of a stratified core upon the nutational motion of the Earth. *Nutation and the Earth's Rotation*, pp. 165-183. Reidel, Dordrecht.

Shen, M., and Zhang, C.Z. 1989. Dynamical evolution of the rotation of Venus. *Earth, Moon, and Planets* **43**, 275-287.

Touma, J., and Wisdom, J. 2001. Nonlinear core-mantle coupling. *Astron. J.* **122**, 1 030-1 050.

Walker, J.C.G. 1975. Evolution of the atmosphere of Venus. *J. Atmos. Sci.* **32**, 1248-1256.

Ward, W. R. 1975. Tidal friction and generalized Cassini's laws in the solar system. *Astron. J.* **80**, 64-70.

Walter, F.M., and Barry, D.C. 1991. Pre- and main-sequence evolution of solar activity. *The sun in time*, pp. 633-657. University of Arizona Press, Tucson.

Yoder, C.F. 1995a. Venus' free obliquity. *Icarus* **117**, 1-37.

Yoder, C.F. 1995b. Astrometric and geodetic properties of Earth and the Solar System. *Global Earth Physics: A Handbook of Physical Constants*, pp. 1-31. American Geophysical Union, Washington D.C.

Yoder, C.F. 1997. Venusian spin dynamics. *Venus II: Geology, Geophysics, Atmosphere, and Solar Wind Environment*, pp. 1 087-1 124. University of Arizona Press, Tucson.

Zahnle, K.J., Kasting, J.F., and Pollack, J.B. 1988. Evolution of a steam atmosphere during Earth's accretion. *Icarus* **74**, 62-97.